INSTITUTO POLITÉCNICO DE LISBOA

Instituto Superior de Engenharia de Lisboa
Escola Superior de Tecnologia da Saúde de Lisboa

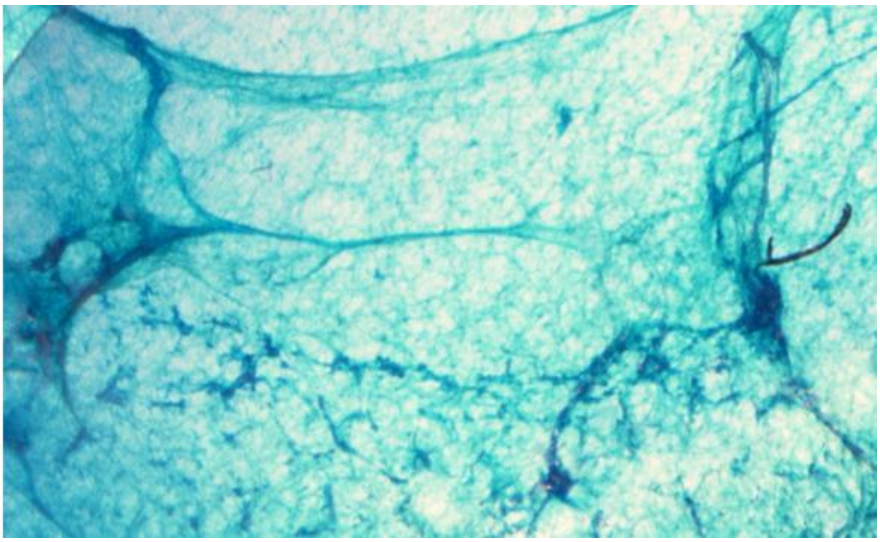

Heparin Functionalization of Fibrin Hydrogels for Tissue Engineering

Jéssica Reais Ramalho

Trabalho Final de Mestrado para obtenção do grau de
Mestre em Engenharia Biomédica

Orientadores
Afonso de Botelho Ferreira Braga Malheiro (Maastricht University)
Cecília Ribeiro da Cruz Calado (ISEL)

Dezembro de 2017

INSTITUTO POLITÉCNICO DE LISBOA

Instituto Superior de Engenharia de Lisboa
Escola Superior de Tecnologia da Saúde de Lisboa

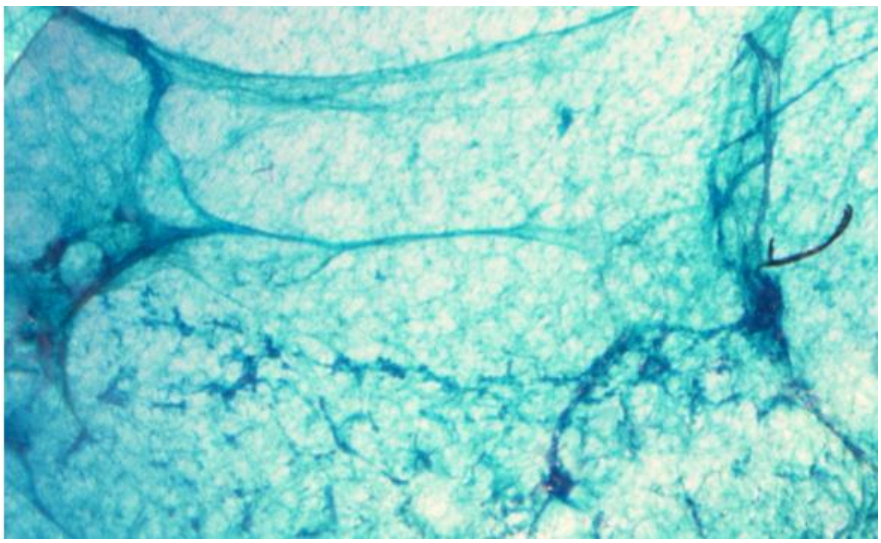

Heparin Functionalization of Fibrin Hydrogels for Tissue Engineering

Jéssica Reais Ramalho

Trabalho Final de Mestrado para obtenção do grau de
Mestre em Engenharia Biomédica

Orientadores
Afonso de Botelho Ferreira Braga Malheiro (Maastricht University)
Cecília Ribeiro da Cruz Calado (ISEL)

Júri

Presidente:	Manuel José de Matos (ISEL)
Vogais:	Ana Margarida Fernandes-Platzgummer (Stem Cell Bioengineering Laboratory, Instituto Superior Técnico, Universidade de Lisboa)
	Cecília Ribeiro da Cruz Calado (ISEL)

Dezembro de 2017

Statement of Original Authorship

I certify that the work in this thesis has not previously been submitted for a degree nor has it been submitted as part of requirements for a degree except as fully acknowledged within the text.

I also certify that the thesis has been written by me. Any help that I have received in my research work and the preparation of the thesis itself has been acknowledged. In addition, I certify that all information sources and literature used are indicated in the thesis.

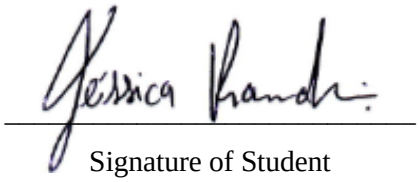

Signature of Student

Statement of Copyright

Sumário

A engenharia de tecidos constitui uma elevada promessa para a completa restauração de tecidos e de órgãos danificados, podendo assim mudar o paradigma da medicina atual. Sendo a base da medicina regenerativa, possui o intuito de revolucionar as formas de melhorar a saúde e a qualidade de vida de milhões de pessoas em todo o mundo, restaurando, mantendo ou melhorando a função dos tecidos e órgãos. Devido ao seu elevado potencial, são já numerosos os exemplos de aplicações publicados, quer em revistas científicas quer nos meios de comunicação normais. De realçar que esta é uma área multidisciplinar com vertentes sociais, económicas, ambientais e éticas, necessitando, portanto, de equipas de profissionais interdisciplinares como da medicina, biologia, química, física, ciências dos materiais, computacionais e de engenharias.

Nas últimas décadas, a engenharia de tecidos tem-se debruçado sobre o desenvolvimento de substitutos capazes de simular histológica, fisiológica e morfologicamente o tecido humano. Esta necessidade surgiu devido à procura de suportes eficazes e seguros para reparação e regeneração de vários tecidos e órgãos vitais; assim como a carência de modelos adequados dos sistemas do corpo humano. Os modelos animais tradicionalmente utilizados para suprimir esta última necessidade não permitem mimetizar com precisão as principais características das patologias humanas, em grande parte devido às diferenças entre as espécies. Em adição, não é possível a aplicação deste tipo de modelos em plataformas de "*high-throughput*", que permitem testar, em paralelo e com rapidez, centenas a milhares de compostos para identificação e seleção dos mais promissores, reduzindo os custos e duração dos ensaios clínicos. Desta forma, o desenvolvimento de novos modelos celulares que mimetizem o tecido humano e patologias associadas de forma mais precisa tem ganho elevado interesse.

Tendo como objetivo mimetizar *in vitro* as características de tecidos humanos, é fundamental ter em conta a organização celular tridimensional (3D) do tecido. Esta configuração 3D deverá permitir a regulação de parâmetros como a disponibilidade de nutrientes ou fatores de crescimento, o stress mecânico induzido pelo sistema de cultura, as interações célula-célula e célula-matriz extracelular, entre outros; pois terá um impacto direto na ativação e direcionamento das vias de diferenciação e funcionalidade celular, conferindo uma maior similaridade entre o modelo e o tecido *in vivo*. Com este propósito, têm sido desenvolvidos sistemas com um maior nível de complexidade, em comparação com as tradicionais culturas em monocamada de células. Entre os sistemas mais utilizados encontram-se as culturas *in vitro* 3D, em que a estratégia passa pela encapsulação das células em matrizes. Estes modelos 3D poderão assim atingir, a longo prazo, a substituição da técnica tradicional de transplantação de órgãos e tecidos, permitir a diminuição da dependência sobre a utilização de modelos animais, e contribuir fortemente para o desenvolvimento de ensaios mais precisos para a avaliação e identificação de novos fármacos, apresentando-se, desta forma, como uma alternativa complementar tanto para a investigação como para a indústria. No entanto, um dos maiores desafios em engenharia de tecidos é a vascularização

e a inervação de tecidos, que permitam o real funcionamento a médio e longo prazo dos tecidos/ órgãos. Para tal, é necessário compreender os desafios relacionados, por exemplo, com a fabricação de uma rede tridimensional funcional de tecidos que permita uma perfusão e difusão adequada para uma boa disponibilização de nutrientes e de oxigénio, para o normal crescimento, diferenciação e proliferação celular. É assim crucial o desenvolvimento de modelos/microambientes 3D envolvendo células, e/ou fatores de crescimento, e que simulem e permitam o teste de biomateriais quanto às suas características vasculares mecânicas, endoteliais e anti-trombogénicas. Para abordar este desafio, o objetivo desta tese foi melhorar as características de um material, que envolvia a conjugação de fibrina com heparina (HCF) e a inclusão de microcanais num hidrogel para aplicações neurais e vasculares. A melhoria de hidrogéis pré-existentes e a adição de microcanais podem promover suportes adequados para engenharias de tecido neural e vascular.

Os hidrogéis são polímeros que através de ligações cruzadas formam uma rede tridimensional hidrofílica de cadeias poliméricas e que absorvem uma quantidade considerável de solvente, devido à sua forte afinidade com a água e com a maioria das soluções aquosas. São considerados materiais fortemente hidratados e são aplicados na regeneração de tecidos como substitutos da matriz extracelular. A sua importância deve-se à semelhança das suas propriedades físicas com as dos tecidos *in vivo*, tais como o elevado conteúdo em água, consistência macia e elástica, e baixa tensão superficial. A fibrina foi o material selecionado de forma a constituir a estrutura suporte do modelo 3D devido à possibilidade de se ajustar a morfologia, propriedades mecânicas e estabilidade do hidrogel controlando a sua concentração. Para além disso, a fibrina é biocompatível, a sua taxa de degradação é controlável e os produtos de degradação não são tóxicos. Quanto à escolha da funcionalização do hidrogel com heparina (HCF, *Heparin-conjugated fibrinogen*), esta foi devido à elevada afinidade da heparina por fatores de crescimento como o fator de crescimento vascular endotelial (VEGF) e o fator de crescimento neural (NGF). A retenção destes fatores pode promover um ambiente ideal para a adesão, migração, orientação e proliferação de células. Para efetuar o estudo do comportamento de células no hidrogel, foram incorporados tenócitos, fibroblastos alongados e especializados do tendão. A sua importância deve-se aos fibroblastos serem células que residem dentro da matriz extracelular de vários tecidos conjuntivos, e que são críticos para a síntese e reparação da matriz. Em resposta a lesões e durante o crescimento tumoral, os fibroblastos são ativados e reconhecidos como miofibroblastos, células de cicatrização de feridas que reparam o tecido danificado através da secreção de colagénio, fibronectina, proteoglicanos, fatores de crescimento do tecido conjuntivo, entre outras proteínas e enzimas. Como sintetizadores e modificadores da matriz extracelular, os fibroblastos também desempenham um papel fundamental no crescimento nervoso e na angiogénese. A angiogénese é a formação de novos vasos sanguíneos a partir de vasculatura existente. O processo ocorre em condições fisiológicas, como por exemplo, durante o desenvolvimento embrionário e cicatrização de feridas; e em condições patológicas, como por exemplo, durante o crescimento tumoral. O processo envolve a ligação de fatores de crescimento como o VEGF, importantes para a proliferação, migração e diferenciação de células, promovendo a formação de novos

vasos sanguíneos. O *electrospinning* foi o método escolhido para a fabricação das microfibras, uma vez que este processo permite obter razões elevadas de área superficial por volume, dimensão de poros adequados às dimensões das células, funcionalização de superfícies e múltiplos locais para interação e conexão celular, e reduzida limitação de fenómenos de transferência de massa. As microfibras foram baseadas em *poly(N-isopropylacrylamide)* (pNIPAM), um polímero termorresistente, mas que apresenta uma temperatura de solução crítica (LCST) de 32°C. Esta característica permite a incorporação das microfibras no HCF e a sua subsequente remoção, originando micro-canalizações. Neste âmbito, é fabricado um hidrogel otimizado com microcanais, o qual pode constituir um modelo biomimético funcional e viável para a promoção de vascularização e de inervação de tecidos. Para alcançar este objetivo, o presente trabalho englobou: (1) o processo de design, fabricação e caracterização do hidrogel, (2) s*eeding* do hidrogel com tenócitos para testar comportamentos celulares e (3) fabricação de microfibras pNIPAM para criação dos microcanais no hidrogel.

Das experiências realizadas observou-se que foi possível ativar e ligar a heparina ao fibrinogénio. Também foi observado que o tempo de gelificação dos hidrogéis aumenta com o aumento da concentração de fibrina conjugada com heparina. Observaram-se dificuldades de polimerização aquando da utilização de 40%, 50%, 75% e 100% de concentração de HCF. Através de análises com o corante azul de dimetilmetileno e de ensaios de imunoabsorção enzimática (ELISA), quantificou-se a heparina e o fator de crescimento VEGF-A dentro do gel e da sua libertação entre 5 e 7 dias, respetivamente. Observou-se que os hidrogéis conseguem reter quer heparina quer VEGF-A. Nos estudos 2D e 3D de incorporação de tenócitos nos hidrogéis de HCF, observou-se a adesão das células em hidrogéis com concentrações de 10%, 35% e 50% de HCF. As melhores configurações de diâmetro e de alinhamento de fibras foram obtidas por *electrospinning* com fibras de 50% pNIPAM em clorofórmio/DMF numa razão de 7:3, bem como de 40% pNIPAM em clorofórmio/DMF numa razão de 3:1. Em termos de perspetivas futuras, sugere-se a continuação da otimização do processo de formação dos hidrogéis de HCF de forma a minimizar as dificuldades de polimerização observadas. Também se sugere uma melhor caracterização dos hidrogéis, especialmente em situações de incorporação de células. Em suma, espera-se que os resultados obtidos no presente trabalho contribuam para o desenvolvimento de modelos biomiméticos neuronais e vasculares, singulares ou combinados, para estudos *in vitro* e aplicações regenerativas.

Palavras-chave:

Engenharia de tecidos, fibrina, heparina, hidrogel, *electrospinning*.

Abstract

One of the greatest challenges encountered in Tissue Engineering (TE) has been the vascularization and innervation of tissues, which allow the medium to long-term functioning of the tissues/ organs. To address this challenge, the goal of this thesis was to optimize the characteristics of a material, involving the conjugation of heparin to fibrin and inclusion of pNIPAM micro-channels in a hydrogel for neural and vascular applications. Improvement of pre-existing hydrogels and the addition of microchannels may promote suitable supports for neural and vascular TE.

Experiments towards the optimization and characterization of heparin-conjugated fibrin (HCF) hydrogels (with gelation kinetics study, alcian blue staining, heparin quantification and VEGF-A release profile), tenocytes seeding to test cell behavior, and fabrication of pNIPAM microfibers for hydrogel microchanneling were conducted. It was observed that it was possible to activate and bind heparin to fibrinogen. It was also observed that the gelation time of the hydrogels increases with increasing concentration of fibrin conjugated with heparin. Polymerization difficulties were observed when using 40%, 50%, 75% and 100% HCF concentration. Through dimethylmethylene blue dye and enzyme-linked immunosorbent assay (ELISA) assays, heparin and VEGF-A growth factor were quantified within the gel and delivered in 5-7 days. It was observed that the hydrogels can retain either heparin or VEGF-A. In the 2D and 3D studies of tenocyte incorporation in HCF hydrogels, cell adhesion was observed in hydrogels at concentrations of 10%, 35% and 50% of HCF. The best diameter and fiber alignment configurations were obtained by electrospinning with 50% pNIPAM fibers in chloroform/ DMF in a ratio of 7:3, as well as 40% pNIPAM in chloroform/ DMF in a ratio of 3:1.

In terms of future perspectives, it is suggested a continued optimization of the HCF hydrogels' formation process in order to improve the acquisition of a consistent HCF product in larger amounts, consequently avoiding the need of constant batch preparation and delay of important and further investigation assays. It is also suggested further characterization of the hydrogels, especially in situations of cells incorporation, to determine with certainty the effect of the fabricated 3D environment in cell behavior. In the future, it is intended to achieve a better usage of the 3D biomimetic models' potential for the repair and regeneration of tissues, as well as the understanding and cure of pathologies; as in specific, the results obtained are expected to contribute to the development of neuronal and vascular biomimetic models, either singular or combined, for in vitro studies and regenerative applications.

Keywords:

Tissue Engineering, fibrin, heparin, hydrogel, electrospinning.

Table of Contents

List of Figures

List of Tables

List of Abbreviations

2D	Two-dimensional
3D	Three-dimensional
BMP-2	Bone morphogenetic protein 2
DAPI	4',6-diamidino-2-phenylindole
DMEM	Dulbecco's Modified Eagle's medium
DMF	Dimethylformamide
DMMB	1,9-Dimethyl-Methylene Blue
ECM	Extracellular matrix
EDC	1-Ethyl-3-(3-dimethylaminopropyl)-carbodiimide
EGF	Epidermal growth factor
ELISA	Enzyme-Linked Immunosorbent Assay
FGF	Fibroblast growth factor
FTIR	Fourier-transform infrared spectroscopy
GAG	Glycosaminoglycans
HCF	Heparin-conjugated fibrinogen
hiPSC-ECMs	Human induced pluripotent cell extracellular matrices
hMSCs	Human Mesenchymal Stem Cells
HUASMC	Human Umbilical Artery Smooth Muscle Cells
HUVEC	Human umbilical vascular endothelial cells
IR	Infrared Resonance
LCST	Lower critical solution temperature
LDH	Lactate dehydrogenase
MES	2-(N-morpholino)ethanesulfonic acid
MR	Magnetic Resonance
NGF	Nerve Growth Factor
NHS	N-Hydroxysuccinimide
NMR	Nuclear Magnetic Resonance
PBS	Phosphate Buffered Saline
PDGF	Platelet-derived growth factor
PEG	Polyethylene glycol
PFA	Paraformaldehyde
PGA	Poly(glycolic acid)
PLA	Poly(lactic acid)
PLGA	Poly(lactic-co-glycolic acid)

pNIPAM	Poly(N-isopropylacrylamide)
SEM	Scanning electron microscopy
TE	Tissue Engineering
VEGF	Vascular endothelial growth factor
WD	Working distance

Acknowledgements

I would like to express my gratitude to Afonso Malheiro, who as my supervisor, teacher and mentor, has taught me more than I could ever give him credit for. He showed me, by his example, what a good ambitious and innovative scientist should be. My biggest thank you for his invaluable guidance, encouragement and generous help.

To Prof. Dr. Cecília Calado, my supervisor from Instituto Superior de Engenharia de Lisboa, who showed her support from the very beginning, and whom I appreciate her valuable time and attention at every stage of my thesis work.

To Prof. Dr. Manuel Matos, for his sincere help and words of encouragement to go ahead in my abroad experience.

To Maastricht University and MERLN Institute for Technology-Inspired Regenerative Medicine, especially to Prof. Dr. Lorenzo Moroni, for giving me the opportunity to carry out an incredible master thesis research experience abroad, in excellent facilities with a tremendous working environment.

To all of those with whom I have had the pleasure to work with during my Erasmus internship. Particularly, to each of the brilliant members of the Complex Tissue Regeneration group who provided me extensive personal and professional guidance, and taught me about both scientific research and life in general.

To all my friends and roommates, who were understanding and great listeners, were there for me during the ups and downs, offered me advices and supported me throughout this entire process.

To my parents, who I admire so much, my biggest thank you for their love, astounding strength and positive energy. I could have not done this without them. Thank you for providing me with unfailing support, both financially and emotionally, and continuous encouragement throughout my academic journey.

To everyone who, directly or indirectly, had an influence and contributed to the completion of my degree.

Maastricht University

Heparin Functionalization of Fibrin Hydrogels for Tissue Engineering

Jéssica Reais Ramalho

2017

This thesis was fully performed under the direct supervision of Afonso de Botelho Ferreira Braga Malheiro (Maastricht University) and Cecília Ribeiro da Cruz Calado (ISEL) in the scope of the Master Thesis in Biomedical Engineering of the Instituto Superior de Engenharia de Lisboa (ISEL) and Escola Superior de Tecnologia da Saúde de Lisboa (ESTeSL).

Chapter 1: General Introduction

1.1. The origin of TE

The dream is as old as humankind. From the earliest documented evidences of ancient civilizations, it is clear that diseases, injuries, death and longevity are among humanity's oldest preoccupations (Weatherall *et al.,* 2006). In recorded history, the desire of restoring damaged human bodies was already noticeable, and tissue and organ regeneration were already reported. Such could be observed in the phrases of Genesis, Chapter II, about the creation of Eve from Adam's taken ribs by the Lord God (Battler *et al.,* 2007). This idea was also manifested in the Greek myth of Prometheus, an individual who was punished by Zeus, enchained to mount Caucasus and tortured perpetually by an eagle who fed from his exposed liver every day after overnight regeneration (Chen *et al.,* 1994). The saint-physicians Cosmas and Damian are also known by the "miracle of the black leg", which is reported to be a successful replacement of a limb and restoration of its lost function in the third-century A.D. (Conolly *et al.,* 2007).

Modern surgery emerged in the final decades of the 19th century as Robert Koch and Louis Pasteur made discoveries that led to conclusions about how a certain germ could invade the body and cause a particular disease. As knowledge about the germ theory of diseases increased, the introduction and development of sterile techniques were carried in concurrency with the development of general anesthetic techniques and control of pain. This enabled courageous surgeons to innovate surgical techniques, saving and improving the quality of human lives by restoring missing functions through the replacement and rebuilding of human body structures (Vacanti, 2007). Techniques such as autografts and allografts have been revolutionary and lifesaving, but major limitations exist. As far as the harvesting of autografts is concerned, the quantity of tissue supply is a problem. The need of surgery at the donor site can also be a problem, since it might contribute to the occurrence of hemorrhages, infections, inflammations, general damages and pain. In the case of allografts, risks of rejection by the patient's immune system are presented, as well as the possibility of disease transmission from the donor to the patient. Also, to the limited allografts available, none were reported with satisfying biological and mechanical properties which secured good segmental reconstruction and replacement (Steven J. Barnes, 2008). These constraints have produced a need for novel therapies, and it is within this context that the field of TE has emerged.

1.2. The emergence of TE

From the previous section, we can conclude that surgically-focused side of the field has a long history; however, inclusion of cells is a more recent development due to the lack of knowledge in molecular cell biology, a field that is only a few decades old. The conciliation of cell biology and experimental surgery is relatively recent and only in this century has TE advanced as a major area of research.

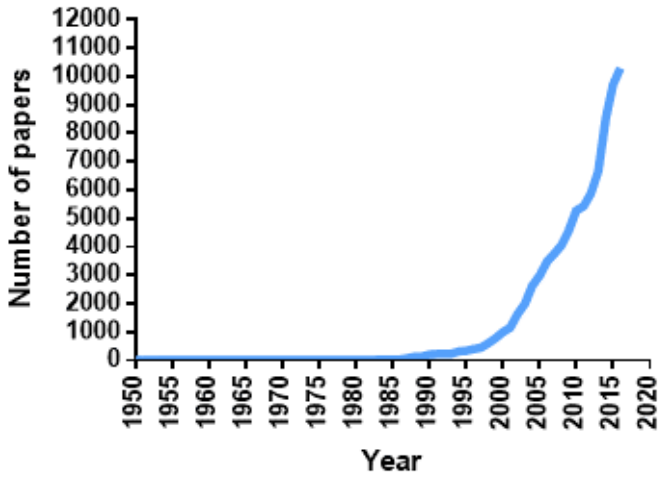

Fig. 1. Growth of TE represented by the number of results returned per year from a Pubmed search for the keywords ”Tissue Engineering”.

As observed in Fig. 1, the field of TE has only started to emerge in the late 1980s. Two broad biological categories in TE can be recognized:

— modification of the growth and functions of cells *in vivo*, and

— construction of bioartificial tissues *in vitro* with or without isolated cells.

The purpose of the first category is the alteration of the growth and functions of cells *in situ*. As an example, it can be referred the case of Erba *et al.* (2010) who studied the neuroregenerative potential of undifferentiated rat adipose derived stem cells to enhance axonal growth and differentiation in a rat sciatic transection model. As for TE *in vitro*, it includes bioartificial tissues (i.e., tissues which are composed of natural and synthetic substances) to be used as an alternative to organ transplantation. Besides their potential clinical use, reconstructed support models (also referred as scaffolds) may also be used as biomimetic tools to study complex tissue morphogenesis and functions in normal and diseased conditions (Berthiaume, 2003). As an example, it can be mentioned the differentiation of rat adipose derived stem cells to a Schwann cell-like phenotype by Georgiou *et al.* (2015), in order to construct an aligned collagen hydrogel to support and guide neurite extension.

1.3. The Biomimetic Tissue Model

One of the main goals of TE, if not the ultimate, follows the approach of the second broad category previously mentioned, and is to create a 3D biocompatible model/scaffold with cell adhesion, proliferation and/or differentiation properties that triggers no inflammatory responses or rejection from the body. Standard fabrication of functional, viable, complex and biomimetic tissue constructs would make a significant difference in Medicine. These could be implanted into defects to correct them, or used as a model to study the tissue response to drugs or in diseased conditions. Hence, it would be able to meet the growing demands for replacing and restoring various tissues and organs. As examples, it can be mentioned the work of Min. *et al.* (2014), who developed a 3D silk protein-based neural culture compatible scaffold, which provided relevant information about brain neural networks and showed capability for the assessment of brain disorders, such as traumatic brain injury. For cell therapy studies, Aratyn-Schaus *et al.* (2016) presented the hypothesis that newly formed myocytes exhibit a weaker contractile strength due to a possible reduction of force transmission between spared and newly formed myocytes. This was tested by creating and using a polyacrylamide hydrogel containing mouse cardiomyocytes to represent a spared myocardium tissue after injury.

1.4. Thesis scope

Although there have been tremendous efforts to replace and restore various parts of the body, most applications have not been successful since the scaffolds were not able to diffuse oxygen and nutrients to support and sustain cellular activity. Successful applications have been limited to thin and avascular tissues such as cartilage and skin, where oxygen and nutrients can diffuse within the constructs and sustain cellular viability. However, as the tissue becomes thicker, the distance between tissue-specific cells and the network grows more than 200 µm (Malheiro *et al.*, 2016), and hence the cells reach hypoxic and apoptotic conditions (Moon & West, 2008). Towards this aim, there have been numerous attempts to induce innervation and vascularization in engineered constructs (Fig. 2).

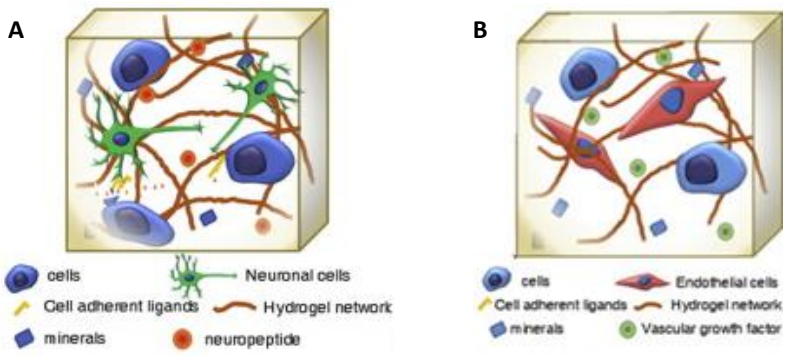

Fig. 2. Vascularized (A) and innervated (B) tissue construct schematic. Adapted from (Marrella *et al.*, 2017).

Looking to understand the process of tissue growth of the vasculature, Doreen et. al created a model that consisted in parallel-arranged hollow polypropylene fibers colonized with endothelial cells (HUVECs) and vascular smooth muscle cells (HUASMCs) (Janke *et al.*, 2013). Another and recent example is the study of Valarmathi *et al*. (2017) to test the possibility of generating a functional vascularized cardiac tissue, through the attempt of vascularization of a collagen scaffold with the interaction between human induced pluripotent stem cell-derived embryonic cardiac myocytes (hiPSC-ECMs) and human adipose-derived multipotent mesenchymal stem cells (hMSCs).

However, a scaffold must have the function of native blood and must provide appropriate mechanical, endothelialization and antithrombogenic properties. Therefore, choosing a proper biomaterial and designing a construct which provides these characteristics is crucial.

To tackle this challenge, this thesis aims at optimizing fibrin hydrogels by heparin functionalization and addition of microchannels, resulting in constructs intended for neural and vascular applications.

Studies of heparin-conjugated fibrin (HCF) hydrogels have already been conducted to form *in vitro* TE models, such as the loading of NGF into HCF gels to form NGF-delivering implants, or the creation of an injectable system for long-term delivery of BMP-2. (Lee *et al.*, 2014; Yang *et al.*, 2010). These two studies mainly provided inspiration, comparison and motivation to this thesis, focusing in the aim of improving and optimizing the fabrication and characteristics of HCF hydrogels.

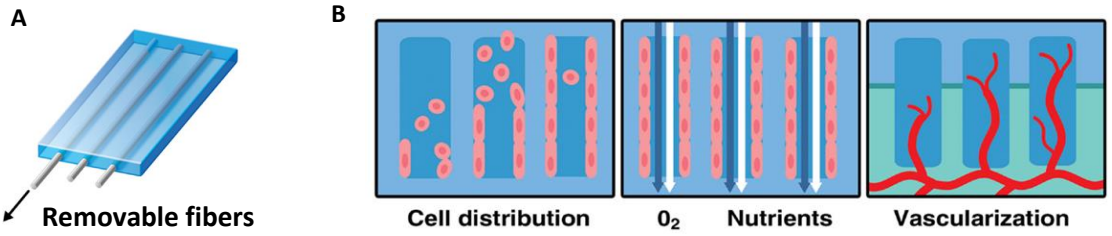

Fig. 3. Embedded fibers in hydrogel (A) and schematic of promotion of vascularization (B). Adapted from (Muehleder *et al.*, 2014).

The optimization of the hydrogels and the addition of microchannels with the purpose of creating space within the hydrogel might allow cells to grow unhindered, the passage of oxygen and nutrients, and facilitate the formation of vessels and/or neurites (Fig. 3). In this way, TE models become excellent supports for neural and vascular growth and orientation.

Fibrin can play the role of scaffold because it promotes cell attachment, cell proliferation, cell migration, exhibits excellent biocompatibility properties and its nontoxic degradation can be controlled. Additionally, fibrin scaffolds are self-assembled into complex polymeric networks with controllable mechanical properties and stability through precursor's ionic strength and concentration. Through the functionalization with heparin, which has high affinity and immobilization properties to capture growth factors such as VEGF and NGF, the release of these might be controlled.

Heparin is a sulfated glycosaminoglycan (GAG) isolated from a variety of natural sources with a strong anticoagulant activity. Combined by glycosidic linkages, it is composed of alternate units of α-D-glucosamine and uronic acid, either α-L-iduronic acid or β-D-glucuronic acid (Dreyfuss *et al.*, 2009). The structure of heparin's chains enables the interaction with a specific range of proteins, allowing the modulation of different cellular processes. Heparin interacts with growth factors and fibrin, which may result in a significant prolonged release of the growth factors locally presented to the cells. Hence, it is possible to achieve an optimal environment for the adhesion, migration, orientation and proliferation of cells (Fig. 4).

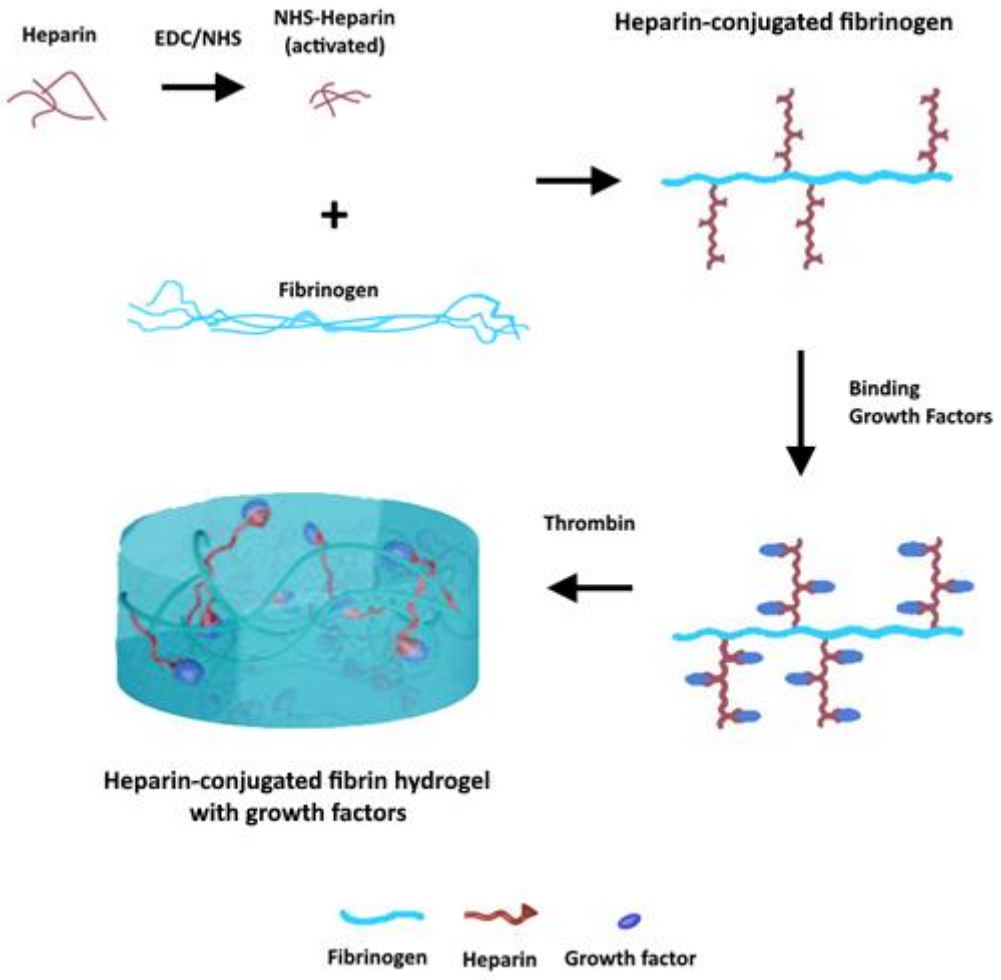

Fig. 4. Schematic of heparin-conjugated fibrinogen hydrogel formation with growth factors. Adapted from (Ma *et al.*, 2015).

Electrospinning was the chosen method for the fabrication of microfibers, since electrospun microfibers may provide large surface area to volume ratios, allowing cell adhesion and proliferation, pore sizes tailored to specific cells dimensions, functionalized surfaces, multiple sites for interaction and attachment, and low mass transfer limitation. As for the microfibers material, pNIPAM is a prominent candidate as thermoresponsive polymer widely known for its lower critical solution temperature (LCST) phenomenon at 32°C in aqueous solutions. Hence, the microfibers may be embedded within the HCF hydrogel and triggered removal achieved by lowering the temperature below the LCST thus forming microchannels.

In this sense, a microchanneled hydrogel to induce innervation and vascularization for a functional and viable construct could be provided.

1.5. Thesis overview

For a better reading experience, this section aims to describe the structure and relevance of each chapter of this thesis. The thesis is divided into six chapters.

Chapter 1 presents a general introduction, which includes the history and importance of the TE field, narrowing to the introduction of biomimetic tissue constructs and the specific thesis scope.

Chapter 2 is specific to tissue constructs, providing enlightenment about the significance of scaffolds in TE, and emphasizing the complexity of the scaffold design process and the need of criterion deliberation (fabrication methods, materials...) according to end applications. The hydrogel formation with Fibrin and the addition of VEGF growth factor are specially highlighted in this chapter.

Chapter 3 introduces Electrospinning by referencing history facts, describing the technique and its importance in the TE field. Important parameters in taking to account in order to obtain an expected electrospun result are mentioned. Smart biomaterials are introduced, with pNIPAM specially highlighted. Finally, the aligned channeling idea is described.

The experimental chapters are presented by chapters 4 (fabrication, characterization of the HCF hydrogel, and tenocytes seeding in HCF hydrogel) and 5 (fabrication of electrospun pNIPAM microfibers). Each of them have a composition of four sections: an introduction to describe and explain the aim of the experiment, a materials and methods section, followed by the presentation of results and a last section for discussion of the results and overall experiment.

Finally, Chapter 6 is reserved for the conclusion of the thesis, by presenting a summary of findings, overall limitations and future perspectives.

Chapter 2: Scaffolds

2.1. Introduction

This chapter aims to review the important properties and fabrication techniques of scaffolds, with special attention to biomaterials selection and cell seeding approaches. Additionally, the specific biomaterials and fabrication methods adopted in the various chapters of this thesis will be highlighted.

Scaffolds are 3D (3D) models, supports, templates or constructs developed to mimic the extracellular matrix (ECM) for new tissue formation and remodeling. The design and fabrication of scaffolds are major areas of biomaterial research.

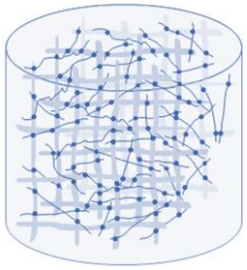

Fig. 5. Hydrogel scaffold schematic. Adapted from (Zheng *et al.*, 2016).

With the progress of the TE field, the need for novel scaffold constructs and fabrication techniques has become of paramount importance. Nowadays, researchers may encounter an enormous variety of scaffold approaches for TE.

The optimal scaffold is one that:

- is formed by a material with controlled biodegradability or bio-resorbability;
- presents appropriate chemistry properties to favor cellular growth, attachment, differentiation and proliferation;
- possesses inter-connecting pores of an adequate size and scale to allow and promote tissue integration and vascularization;
- has adequate mechanical properties to match the specific extracellular matrix environment in study;
- does not induce any negative biological response;
- is easily fabricated in diverse shapes and sizes to fulfill several application needs (Liu *et al.*, 2007; Sachlos *et al.*, 2003).

2.2. Materials

One of the first considerations when designing a scaffold for TE is the choice of the material. The three main material types which have been successfully investigated to be applied in developing scaffolds include:

- natural polymers,
- synthetic polymers, and
- ceramics (Willerth & Sakayama-Elbert, 2007; Radulescu *et al.*, 2007).

However, polymers show more versatility and similar structural characteristics of the ECM, and that is why they are the main material type which has been the most successfully investigated to be applied in overall developing scaffolds. Polymers can be divided into natural or synthetic polymers of according to their source (Chen *et al.*, 2013). Natural polymers' main advantage is that they are similar to organic constituents and are recognized by the host cells in order to give rise to positive cellular interactions. However, natural polymers present variability between batches, being their composition variable according to the extraction source and, in addition, because of the potential risk of immunogenicity, they need to undergo a purification process before being applied (Willerth & Sakiyama-Elbert, 2008). Synthetic polymers have the advantage of being obtained by controllable chemical processes. These are usually simple and allow large-scale production without variations between batches, and make it possible to shape some characteristics such as degradability, and mechanical properties of the formed network, according to the characteristics of the tissue to be replaced (Willerth & Sakiyama-Elbert, 2008).

2.2.1. Natural Polymers

Within the natural polymers, three groups can be distinguished: polysaccharides, polynucleotides and polypeptides (Yadav *et al.*, 2015).

Alginate is a polysaccharide extracted from algae. Structurally, it is a linear copolymer composed of α-L-guluronic acid units and β-D-mannuronic acid linked by bonds (1 → 4). Due to its biocompatibility, low toxicity, ease of gelling and low cost, this polysaccharide was chosen to be used in many applications in the biomedical area. In tissue regeneration, alginate has been applied in the regeneration of bone (Rubert *et al.*, 2012; Zhao *et al.*, 2010), cardiac (Dahlmann *et al.*, 2013), cartilage, and skin tissue (Slaughter *et al.*, 2009; Straccia *et al.*, 2015). As an example, is the study of Dahlmann *et al*. (2013) related to the modification of physical and mechanical properties of the hydrogels. Through this study, it was found that the scaffold properties could be adjusted with the derivatization, change in the concentration and composition of blended polymers (alginate and hyaluronic acid). It was also

observed that the addition of collagen allowed adhesion, proliferation and integration of the cells into the formed matrix, allowing the formation of a new tissue with characteristics similar to myocardium. Hence, it was observed that the blended polymers had a great potential of its general properties adjustments, allowing the optimization of the matrix so as to better mimic the myocardium.

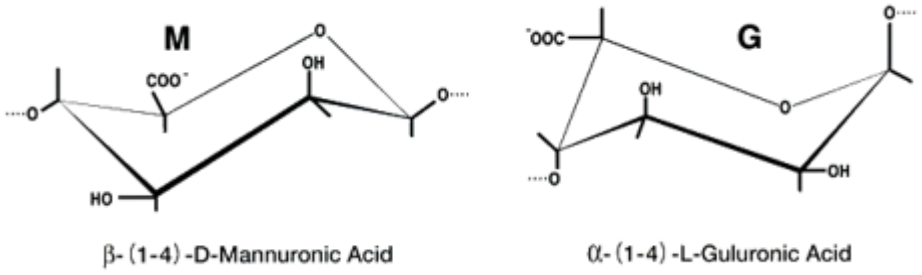

Fig. 6. Chemical structure of alginate. From "Chemical Structure « Alginate « KIMICA corporation | manufacturer and world-wide supplier of "Alginate / Alginic acid" Alginic Acid, Propylene Glycol Alginate, Calcium Alginate, (2017)".

Chitin is the second most abundant natural polymer on planet Earth, right after cellulose, and it can be found in the exoskeleton of insects and crustaceans. Structurally, it is presented as a linear chain polysaccharide composed of glucosamine monomeric units and β-linked N-acetyl-D-glucosamine units (1 → 4). From chitin's deacetylation, chitosan can be obtained, which presents a higher proportion of glucosamine units compared to chitin (Laranjeira & Fávere, 2009; Synowiecki & Al-Khateeb, 2003).

Both chitin and chitosan present no toxicity and have biodegradable, biocompatible and low immunogenic properties. However, unlike chitosan, chitin is insoluble in most solvents due to the hydrogen bonds it possesses (Pillai *et al.*, 2009). Hence, chitosan has been the one most used and applied in TE not only because of the previous mentioned properties, but also because of its hydrogel formation capacity. Through the study of Levengood and Zhang (2014), it was recognized chitosan's potential for bone TE. Chitosan allowed the adhesion and proliferation of osteoblasts and the formation of a bone matrix mineralization. Lisková *et al*. (2015) also studied the application of chitosan to bone regeneration by developing injectable chitosan hydrogels containing sodium and magnesium glycerophosphate. The hydrogels demonstrated cytocompatibility and the potential for this application.

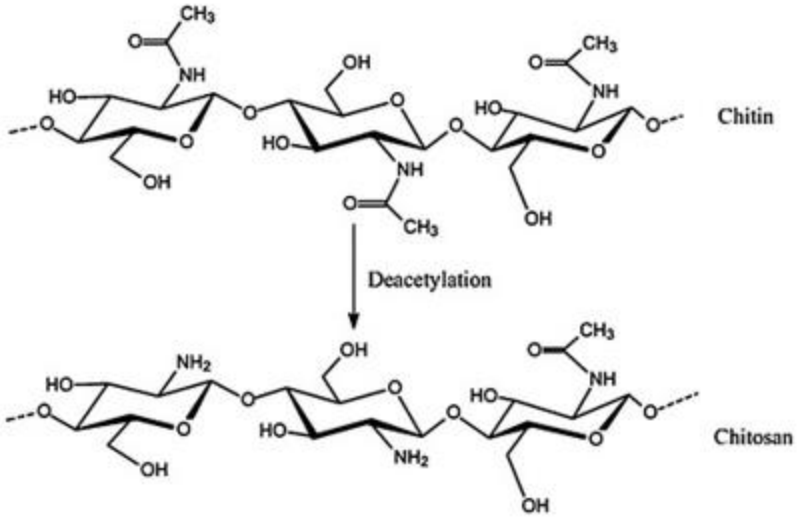

Fig. 7. Chemical structure of chitin and chitosan (obtained after chitin's deacetylation). From (Zuber *et al.* 2013).

Collagen is the most widely used natural polypeptide polymer. Its composition is denoted by a family of proteins composed of three polypeptide chains arranged as a triple helix. There are more than twenty types of collagen (Gelse *et al.,* 2003), and among these, the most abundant are collagen type I and III. Collagen hydrogels can be formed by physical crosslinking or chemical crosslinking. They are thermally reversible when they are obtained by physical crosslinking. This polymer can present some limitations, being necessary the optimization of some characteristics according to the tissue that is intended to regenerate. Since it presents a high rate of degradation, its hydrogels will have less stability and reduced mechanical resistance. The disadvantages of these hydrogels are that they are potentially immunogenic, require a costly purification process, present a high rate of degradation, low signs of mechanical strength and, hence, low stability. However, collagen has still been widely used in TE due to its biocompatible and biodegradable properties.

As an example, Ma *et al.* (2016) prepared a hydrogel containing collagen, hydroxyapatite and alendronate, a drug used for the treatment of osteoporosis. The hydrogels were synthesized using as an organic compound named genipine as a crosslinking agent. Hydrogels with different ratios of hydroxyapatite and alendronate were prepared and the results obtained were compared. The hydrogels presented biocompatibility, biodegradability and good mechanical properties, and these could be adjusted through the modification of hydroxyapatite and alendronate proportions, and also through the alteration of the crosslinking agent's concentration. In resume, these hybrid hydrogels promoted cell adhesion and proliferation in this in vitro study, and showed potential for application as bone scaffolds for TE.

Fibrin is a natural polymer obtained from fibrinogen, a large, complex and fibrous glycoprotein protein in plasma which has a key role in many biological processes such as hemostasis, inflammation, wound healing and angiogenesis. It is composed of two sets of three polypeptide chains (Aα, Bβ, and γ). It also includes two fibrinopeptides connected by 29 disulfide bonds within the E domain, A and B. One and two interchain disulfide bond(s), respectively, link α and γ chains to the same chains of the opposite subunit. Via a disulfide bond, the β chain of one subunit is linked to the α chain of the other subunit. In the other hand, a second β chain is connected to the γ chain of the opposite subunit via an additional disulfide bond. Hence, the two β chains are not directly linked to each other. The fibrinogen protein is approximately 45 nm long and it contains two identical outer D domains, each connected to the central E domain, which contains the two pairs of fibrinopeptides, by a coiled-coil segment (Noori *et al.*, 2017).

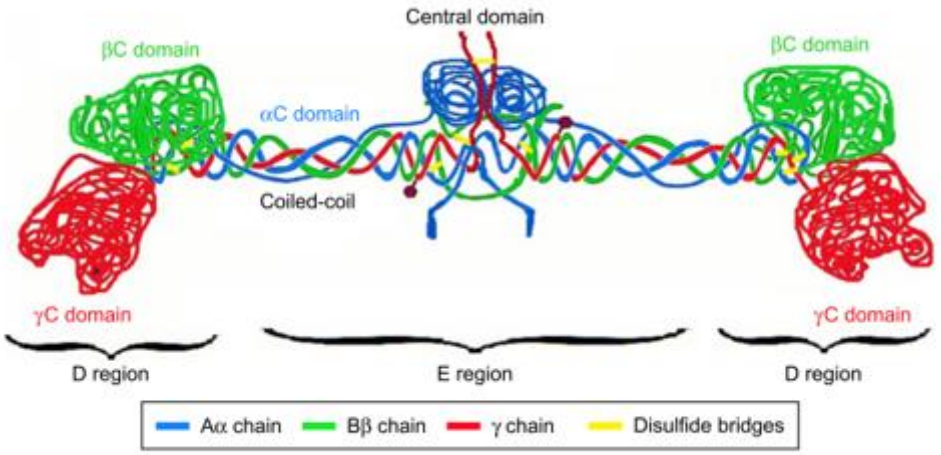

Fig. 8. Fibrinogen's structure. Aα chains are shown in blue, Bβ chains are shown in green and γ chains are shown in red. Disulfide bridges stabilizing the coiled-coil regions are shown in yellow. Adapted from (Noori *et al.*, 2017).

Fibrin is an ideal candidate for TE applications since it possesses remarkable advantages over other biomaterials (Noori *et al.*, 2017). Fibrin gels are rapidly assembled by a modified polycondensation reaction from fibrinogen. Fibrinogen removes the part of the fibrinogen polypeptides that prevent its spontaneous polymerization as soon as the clotting enzyme thrombin is activated in the clotting cascade (Janmey *et al.*, 2009).

The clotting/coagulation cascade is composed by reactions that initiate after blood contact with a foreign material or upon injury (Schenone *et al.*, 2004). Thrombin is the protease generated in the last step of the clotting cascade that cleaves short peptide strands from the central region of the fibrinogen molecule into fibrin monomers.

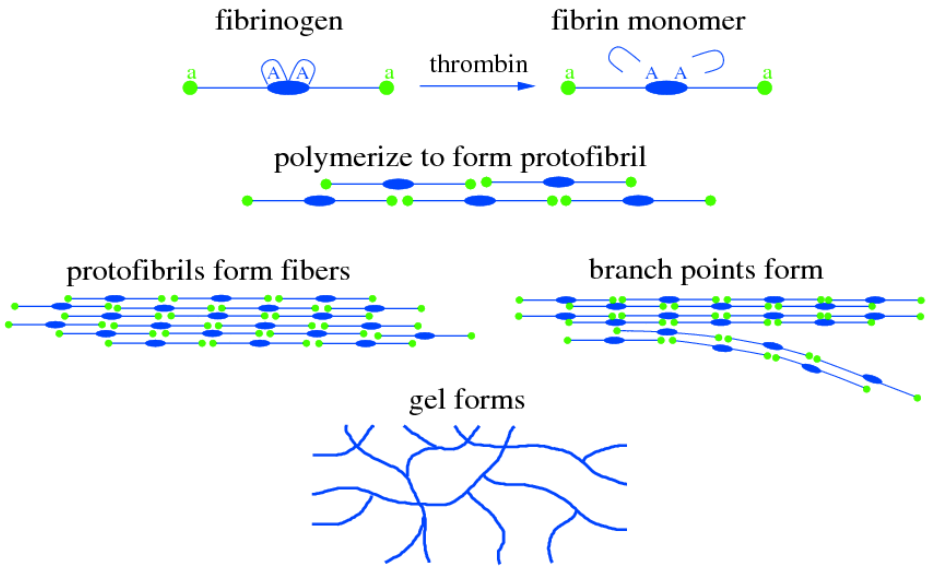

Fig. 9. Schematic of fibrin polymerization. Adapted from (The University of Utah, 2017).

These monomers spontaneously associate together into long strands called protofibrils which can perform a lateral assembly of thicker fibers branches when sufficiently long. As a result, gelation occurs, and a 3D fibrin network is obtained (Fig. 9).

Fibrin possesses multiple interaction sites for cells and other proteins and its properties can be controlled by manipulating polymerization conditions such as pH, ionic strength and modifying the concentrations of the precursors (fibrinogen and thrombin) solutions, an important feature for scaffolds design (Noori *et al.*, 2017). The modification of polymerization parameters also affects biochemical cues in fibrin, such as the concentration and distribution of ECM ligands, cytokines, and growth factors. These may affect the properties of cell growth, proliferation, differentiation, and expression of growth factors. Cell behavior may also be affected by physical cues such as matrix stiffness (Reinertsen *et al.*, 2014). Hence, fibrin is allowed it to act as a bioactive matrix, becoming suitable for cell functionality, delivery and support.

2.2.2. Synthetic Polymers

In the synthetic group, countless polymers are included, and the most widely used in TE are polylactic acid (PLA), polyglycolic acid (PGA) and poly (ethylene glycol) (PEG).

Poly (ethylene glycol) (PEG), also known as poly (ethylene oxide), is a biocompatible, with high permeability hydrophilic polymer, that has low immunogenicity and allows the diffusion of nutrients (Lin & Anseth, 2009; Slaughter *et al.*, 2009). Due to these properties, it has been used in

biomedical applications such as scaffolds for the development of new tissues and matrices for the controlled release of biomolecules (Lin & Anseth, 2009). In the field of TE, PEG is used for the formation of hydrogels with highly swelling capacity, resulting in a high-water content construct with viscoelastic properties similar to soft tissues. This creates an environment similar to the extracellular matrix (Papavasiliou *et al.,* 2012) and adequate to cellular applications. The advantages of this polymer are the possible chemical modifications in order to change some of its characteristics, such as mechanical resistance. (Lin & Anseth, 2009).

Dahlin *et al.* (2014) evaluated the attachment and viability of human fibroblasts to test the influence of the modification of the hydrogels with argininaglycine-aspartic acid in adhesion and cell survival. The hydrogels were formed with three different in vitro degradation times (28, 60 and 120 days), with or without addition of the arginine-glycine-aspartic acid sequence. Cell viability was determined by measuring the concentration of the enzyme lactate dehydrogenase (LDH), a cell membrane breakpoint marker. After 13 days of the beginning of the study, a decrease in the number of cells in all the hydrogels studied was visualized, and the hydrogels with a degradation time of 60 days showed a higher LDH value than the rest.

In conclusion, all PEG formulations studied showed a similar behavior, except formulations with a degradation rate of 60 days. Hence, there is a possibility of applying PEG hydrogels to guided bone regeneration, however, it is necessary to optimize the degradation time of the hydrogel (Dahlin, Johansson, Hoffman, & Molenberg, 2014).

The polyglycolic acid (PGA) is a rapidly degradable polymer with a glass transition temperature from 35 to 40°C. In the other hand, the polylactic acid polymer (PLA) has a higher glass transition temperature between 60 and 65°C, and has an additional methyl group which gives it greater hydrophobicity and stability to hydrolysis. The acopolymer formed by units of polylactic acid and polyglycolic acid is called polylactic-co-glycolic acid (PLGA) (Ulery *et al.*, 2011). It is the synthetic polymer most frequently used for bone regeneration, and can be developed in the form of scaffolds, coatings, fibers or microspheres (Félix Lanao *et al.*, 2013). It has the advantage of being composed of the two polymers, presenting a combination of both properties, and these are open to optimization through changes in the proportion of each polymer (Ulery *et al.*, 2011).

As an example, the hydrogel composed of PLGA and PEG created by Yan *et al.* (2015) can be mentioned. A heat-sensitive PLGA-PEG-PLGA hydrogel loaded with simvastatin was developed for bone regeneration applications. Simvastin has an effect on the differentiation and mineralization of osteoblasts, having a positive effect on the formation of bone tissue (Walter *et al.,* 2014; Yang *et al.*, 2011), hence why the loading of this drug was decided by the authors. The hydrogels were synthesized

with and without simvastatin, and in vitro and in vivo studies were performed using a mouse derived osteoblast cell line (MC3T3-E1). Cell proliferation and differentiation were observed, with higher mineralization and expression of the osteogenic gene in the case of the hydrogel loaded with simvastatin. Bone formation was found in tibial defects injected with PLGA-PEG-PLGA hydrogel containing simvastatin, compared to the hydrogel without simvastatin and control. In conclusion, the results obtained points that the application of PLGA-PEG-PLGA hydrogels containing simvastatin could be used as a therapeutic alternative for bone tissue regeneration (Yan *et al.*, 2015).

2.3. Growth Factors

Growth factors are signaling molecules that control a variety of cellular functions (Vo *et al.*, 2012) such as growth, proliferation and migration (Zhao *et al.*, 2015). As previously mentioned, scaffolds are intended to mimic the natural ECM's structure, surface morphology and chemistry properties to achieve improved cell-matrix interactions and new tissue formation. The delivery of growth factors from a scaffold is an attractive strategy for TE, since growth factors, if properly integrated in the 3D system, may be able to directly stimulate cellular activities. Hence, besides its structural purposes, the scaffold serves as a delivery carrier for the controlled release of growth factors.

Some growth factors are small peptides called cytokines, but only those affecting cell growth and differentiation signaling pathways are the ones considered as growth factors. (Stone & Bhimji, 2017). Vascular endothelial growth factor (VEGF), platelet-derived growth factor (PDGF), fibroblast growth factor (FGF) and epidermal growth factor (EGF) are examples of protein growth factors.

The vascular growth factors play a significant role in physiological and pathological angiogenesis (Dvorak *et al.*, 1995). Several molecules that stimulate angiogenesis have been identified, however, we will focus on VEGF, since it was the growth factor chosen to work with in this thesis. VEGF acts essentially on the regeneration of vascular tissue, but it also assists in the regeneration of nerves, since during the regeneration process, there is a close relation between the nerve fibers and the blood vessels. The blood vessel infiltration in nerve conduction chambers is significantly increased by the addition of VEGF, consequently increasing the Schwann cells migration and axonal regeneration (Hobson *et al.*, 2000; Terenghi *et al.*, 1995). VEGF can also act as a neuroprotectant in neurons *in vivo* and *in vitro* after ischemic injury (Wongtrakul *et al.*, 2002). There is evidence that this growth factor has neuroprotective and neurotrophic effects on neuronal and glial cells not only in culture but also in vivo, hence possibly stimulating and promoting stem cell survival and proliferation (Jin *et al.*, 2000).

VEGF showed to have a significant role in the response to cerebral and peripheral ischemia, since it is capable of promoting nerve repair after traumatic spinal cord injury.

As an example, the study of Wongtrakul *et al.* (2002) about the effect of VEGF on conventional nerve grafts' angiogenesis and neovascularization can be mentioned. A 2.5 cm segment was removed from the sciatic nerve and orthotopically repaired. After 3 days, a significant percentage of the control nerves and all the nerves treated with VEGF presented signs of partial longitudinal neovascularization. Other studies have investigated the effects of VEGF on rat sciatic nerve regeneration in vivo. The grafts were pretreated with VEGF, NGF or laminin prior to implantation. Grafts pretreated with VEGF stimulated the growth of Schwann cells and blood vessels, but not axons. This work points towards the relevance of local application of VEGF to promote the proliferation of Schwann cells and neovascularization, both very important during nerve regeneration (Zachary, 2005).

To mimic the ECM behavior and achieve a viable functionality of tissues in the long-term, efforts to control the retention and release of growth factors have engaged several biomaterial approaches including strategies of ionic complexation, covalent conjugation, affinity binding or physical entrapment of growth factors within polymer scaffolds (Vo *et al.*, 2012).

In this thesis, the strategy of functionalizing fibrin with heparin in order to take advantage of the polysaccharide's high affinity properties was applied. The chains of heparin are known to interact with a variety of proteins such as heparin-binding growth factors (e.g. VEGF and NGF), morphogens, pathogens, extracellular matrix components, among many others. The heparinization is a crucial step of the HCF hydrogel formation to enable a prolonged and controlled bioactivity and release of the growth factors, as well as GFs' protection from proteolytic degradation (Jha *et al.*, 2015). Consequently, an optimal environment for the adhesion, migration, orientation and proliferation of cells may be achieved.

Chapter 3: The Electrospinning Technique

3.1. Introduction

In recent decades, the electrospinning technique, also known as electrostatic spinning, has attracted great interest due to its capability of processing a vast range of polymeric materials in form of nanofibers in an easy and effective manner (Zhang *et al.*, 2017). The significance of nanofibers comes from the inherent properties such as the extremely high surface to volume ratio, and the engineered properties such as fiber diameter, porosity, stability, hydrophilicity, and permeability. There are various processes for nanofiber fabrication available, such as self-assembly and phase separation. However, electrospinning shows versatility and flexibility in terms of material selection and control over fibers' morphology and diameter, which is why this technique is regarded as the most attractive for designing of natural and synthetic polymer-based nanofibers for TE (Naves *et al.*, 2017; W. Zhang *et al.*, 2017). In addition, it has the possibility of forming various fiber network patterns, including aligned, nonwoven or custom-patterned fiber meshes, three dimensional (3D) structures, among others. These characteristics make electrospun microfibers elected for applications in sensors, energy, biomedicine, among others (W. Zhang *et al.*, 2017).

3.2. History

The electrospinning technique was discovered and described as a derivative of electrospraying, a method that utilizes electrostatic forces to generate polymer droplets. Geoffrey Taylor published a study in 1964 which explained, in the presence of an electric field, the deformation of water droplets. He was able to demonstrate the distortion of spherical drops into conical shapes through his mathematical reasoning. In 1969, another article of his own was published focusing on the formation and ejection of fine jets from viscous solutions. In the late 1970s, Annis *et al.* (2016) investigated specifically for potential vascular prostheses but, overall, the electrospun polyurethane fibers obtained were not considered to have many useful applications. The technique grew weak for many years until the early 1990s. Interest was renewed mainly because of the need for a process which would enable the fabrication of fibers at the nanometer scale. In this way, many researches such as Reneker and Yarin (2016) began to examine the fibers that were formed attention by this process with a more precise and investigate the physics conducting their formation.

3.3. The Process

To produce fibers, two standard set-ups, vertical and horizontal, are currently available. Both consist of four major components: a high-voltage power supply, a syringe with a metallic needle, a syringe pump and a grounded collector (Fig. 10). Through the syringe, a polymer solution is dispensed at a constant rate into a high voltage electrical field generated between the end of the needle and the collector. As it is dispensed a polymer solution droplet forms at the end of the needle tip, which when subjected to the electrical field, elongates into a conical shape named Taylor cone. When the repulsive electrical forces overcome the surface tension forces, an electrified polymer jet ejects from the apex of the cone. The jet is then elongated and whipped continuously by electrostatic repulsion forces. Therefore, the electrospinning process is conducted by a variety of forces between charges on the jet surface, e.g. the viscoelastic force of the solution, the surface tension, the electrostatic force due to the external electric field, and the gravitational force (Sapountzi *et al.*, 2017).

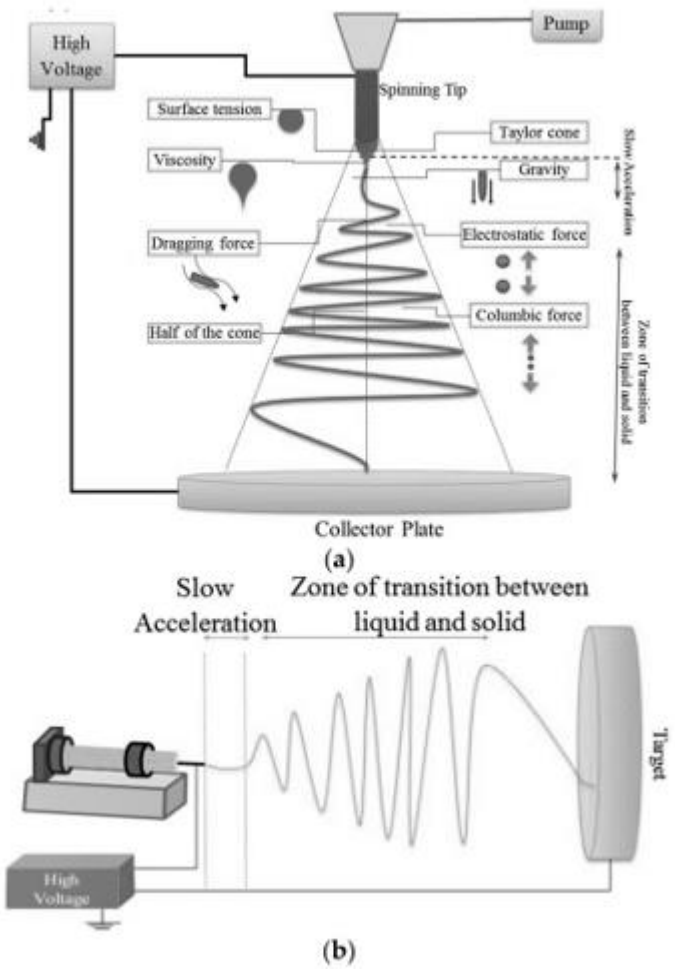

Fig. 10. Schematic of electrospinning in typical horizontal (a) and vertical set-ups (b). From (Sapountzi *et al.*, 2017).

The technique is highly versatile since, besides the conventional non-oriented fibers, a variety of morphologies (e.g. fiber diameter…) and structures (e.g., aligned or crossed fiber arrays, ribbon, necklace-like, nanowebs, hollow, helical or coil fibers…) can be obtained by modifying electrospinning conditions or set-up (e.g., polymer concentration, voltage, flow rate, distance between capillary and collector…) (Sapountzi *et al.*, 2017) (Fig. 11).

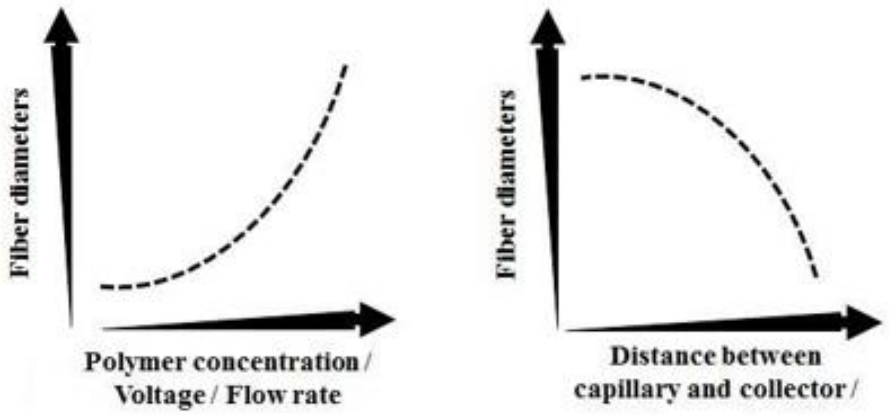

Fig. 11. Fiber diameter in proportion to polymer concentration, voltage or flow rate (A), and fiber diameter in proportion to distance between capillary and collector (B). From (Sapountzi *et al.*, 2017).

3.4. Materials

The choice of polymer represents a key component in the development of sustained release electrospun fibers. The seemingly unlimited number of natural and synthetic polymers that can be electrospun highlights the versatility of this platform. Therefore, the intended application for the sustained release fibers often dictates the polymer selection. Both non-biodegradable and biodegradable polymers have been used for sustained release from electrospun fibers (Chou *et al.*, 2015). To date, more than 200 polymers have been successfully electrospun to nano-scale or micro-scale fibers, including natural materials (e.g., collagen, gelatin, hyaluronate (HA), chitosan, silk fibroin (SF), etc.) and synthetic materials (e.g., polycaprolactone (PCL), poly-L-lactic acid (PLLA), poly(lactide-*co*-glycolide) (PLGA), polyethylene oxide (PEO), etc.) (Kong & Mi, 2016).

3.4.1. Smart biomaterials and pNIPAM

Stimuli-responsive polymers, also known as “smart” polymers, demonstrate rapid changes in their microstructure from a hydrophilic to a hydrophobic state, once triggered by changes in the environment. External stimuli such as heat, pH, ionic strength, magnetic and electric fields, light, ultrasound, and chemical species trigger changes in the environment. The system is capable of returning to its initial state when the trigger is removed because the macroscopic changes are reversible (Panambur *et al.*, 2017). The use of the terms “smart” and “intelligent” to describe the materials came from the USA. The smart materials had been around for decades, but the use of the terms only started in the 1980s. Early applications of these materials started with technologies that involved the use of nickel as a sonar source during World War I to find German U-boats by Allied forces (Badami & Ahuja, 2014). Smart biomaterials have been around for many years and they have found many applications ever since. In this thesis, we will focus on pNIPAM, which was the chosen polymer for the fabrication of microfibers.

Poly(N-isopropylacrylamide) (pNIPAM) is one well studied smart biocompatible and temperature responsive polymer, which exhibits a lower critical solution temperature (LCST) at 32°C. At temperature above the LCST, the intermolecular hydrogen bonding between the pNIPAM chains and water molecules is replaced by intramolecular hydrogen bonding between CO and N–H groups along the pNIPAM chains. This results in compact and collapsed chains that interact minimally with water and, thus, exhibit hydrophobicity. In contrary, the ionic moieties interact strongly with the media below the LCST, and result in hydrophilicity (Patra *et al.*, 2016).

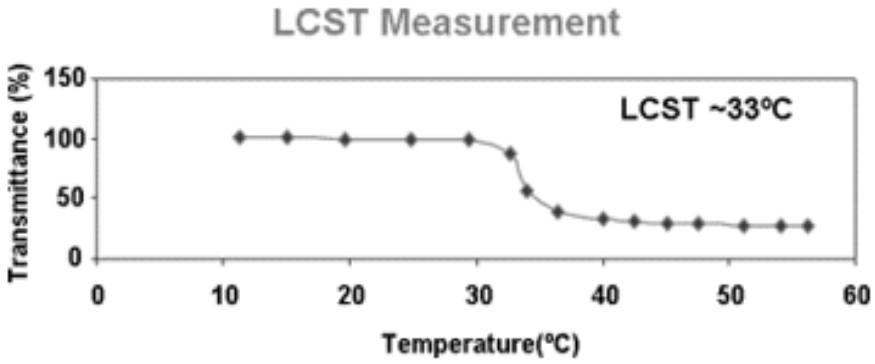

Fig. 12. Plot of transmittance as a function of temperature for P(N-isopropylacrylate-co-5% methacrylic acid) , 1% aqueous solution, pH = 4.46. From (Panambur *et al.*, 2017).

3.5. Parameters

One of the great advantages of electrospinning is that the morphology of the electrospun nanofibers can be easily controlled by changing the parameters during the electrospinning process (Chen *et al.*, 2017). Many processing parameters such as:

- the chemical nature of the polymer solution (molecular weight, solvent and concentration);
- the applied voltage;
- the distance between the syringe needle tip and the collector;
- the flow rate;
- the humidity and,
- the temperature may affect the morphology of the fibers (Kong & Mi, 2016).

The concentration of the polymer is an important parameter since it determines the morphology of the electrospun fibers. The surface tension can be as dominant as the polymer concentration decreases. In addition, solution viscosity is another critical parameter, as it determines if the polymer can be electrospun into fibers or not. The solution viscosity is highly dependent on the concentration and the molecular weight of the polymer used. In principle, a polymer with higher molecular weight has, on average, longer molecular chains. Thus, it will form more entanglements which will lead to a higher viscosity of the polymer solution. In the case of solutions prepared with high molecular weight polymers, if the polymer concentration is low, it still can produce a uniform jet due to a sufficient level of solution viscosity. In the opposite hand, if the molecular weight is too low, even with a high polymer concentration, an appropriate polymer solution viscosity cannot be guaranteed. The polymer will tend to form a bead structure on the collector. Processing conditions such as applied voltage and flow rate also play a significant role in fiber formation during electrospinning (Chen *et al.*, 2017).

3.6. Aligned Channeling

In concern to vascular and neural regeneration, scaffolds with high alignment exhibit impressive advantages in terms of their mechanical properties and cell proliferation processes, such as cell orientation, migration, and differentiation. Highly-aligned fibers play a crucial role in neurite outgrowth of the neural cell when compared to randomly-distributed fibers (Chaurey *et al.,* 2012; Yang *et al.,* 2005). Neurite outgrowth, cell migration and the extracellular matrix deposition of the neural cells on the aligned fibers tend to stretch in a parallel direction along the alignment of the nanofibers (Huang *et al.,* 2015; Jha *et al.,* 2011; Kim *et al.,* 2016; Zhao *et al.,* 2011).

A way to create longitudinally oriented channels is to create a construct from one polymer with embedded aligned oriented fibers from another polymer, and then selectively dissolve the fibers to form oriented channels (Biazar *et al.,* 2010). As an example, the study conducted by Yu *et al.* (2005) can be mentioned. It involved HEMA, which was copolymerized with ethyl methacrylamide (AEMA) to create a P(HEMA-co-AMEA) gel. PCL fibers were embedded in the gel, and then selectively dissolved by acetone with sonication to create channels. When compared with scaffolds without channels, the addition of 82–132 channels could provide an approximately 6-9 fold increase of surface area, which is advantageous for regeneration studies that depended on contact-mediated cues (Yu & Shoichet, 2005).

Chapter 4: Fabrication and Characterization of HCF Hydrogel

4.1. Materials and Methods

4.1.1. Synthesis of heparin-conjugated fibrinogen

N-Hydroxysulfosuccinimide sodium salt (NHS, 5 mM, Sigma-Aldrich, 56485) and N-(3-Dimethylaminopropyl)-N′-ethylcarbodiimide hydrochloride (EDC, 2 mM, Sigma-Aldrich, E1769) were dissolved in a 2-(N-morpholino)ethanesulfonic acid buffer solution (MES, 0.1M, pH 6.5, Sigma, M3885). Immediately, 0.1% w/v of heparin sodium salt from porcine intestinal mucosa (Sigma, H3149) was dissolved in the previous solution and reacted for 30 m at room temperature (RT) under agitation for activation of the heparin's carboxylic acid groups. 0.1% w/v of fibrinogen from bovine plasma (Sigma, F8630) was added to the resultant solution and left to react overnight at RT. The resultant heparin-conjugated fibrinogen (HCF) product was recovered through precipitation with large excess acetone anhydride, centrifugation at 20ºC and 7874 rpm speed for 35 m, followed by vacuum drying for 24 h at 20ºC. The resultant dried product was dissolved in phosphate buffered saline (PBS), dialyzed through a Spectra/Por® 7 dialysis membrane tubing (MWCO of 25 kDa, Spectrum) for 24 h in MilliQ water at 4ºC (with water changes every 2-4 h), and lyophilized for 48 h.

4.1.2. Preparation of samples for ^{1}H-NMR spectroscopy

Samples of (1) pure fibrinogen, (2) activated heparin and (3) HCF were prepared by dissolving 7 mg of each product in a solution of deuterium oxide. The ^{1}H-NMR spectra were recorded on a NMR Bruker Ascend 400/Avance III spectrometer and analyzed in TopSpin 3.5pl7 software.

4.1.3. Preparation of samples for FTIR spectroscopy

5 mg of (1) pure fibrinogen, (2) activated heparin and (3) HCF were reserved, enough to cover the spectrometer's sample compartment. The FTIR spectra of the samples were recorded on a FTIR Nicolet iS50 spectrometer.

4.1.4. Formation of modified fibrinogen matrices in different concentration ratios

10.5 mg/ml of pure fibrinogen and 10.5 mg/ml of HCF were prepared and mixed 1:1 with a thrombin solution (10U/ml plus 5mM calcium chloride). The matrices were prepared in the following percentages: 0%, 10%, 40%, 50%, 75% and 100% of HCF; with a total volume of 200µl in a 48-well

microplate. Immediately, the solutions were gently mixed to disperse them homogeneously trough the well and avoid bubble formation. Thereafter, the plate was incubated at 37ºC until gel formation.

4.1.5. Tracking of matrices' gelation time

In order to track the matrices' gelation speed, the samples were observed every 15 minutes. The gelation time of each sample was registered. After gel formation, the samples were covered in a volume of 500 µl of Phosphate Buffered Saline (PBS) for gel hydration.

4.1.6. Staining of matrices with Alcian Blue

An alcian blue dye solution (pH 2.5) was prepared by adding 1 g of Alcian Blue to 100 ml of 3% Acetic Acid. After the removal of PBS from the samples, the dye solution was added to each sample and left at RT for 30 m. The staining solution was removed and the wells washed with PBS until the PBS washing solution became clear. Sample images were captured with a Nikon SMZ25 stereomicroscope.

4.1.7. Heparin quantification with 1,9-Dimethyl-Methylene Blue (DMMB)

Three solutions in PBS of the following products were prepared: (1) fibrinogen (10.5 mg/ml) with non-conjugated heparin (6.75 mg/ml), (2) modified (heparin-conjugated) fibrinogen (10.5 mg/ml) before dialysis, and (3) modified (heparin-conjugated) fibrinogen (10.5 mg/ml) after dialysis. To prepare DMMB dye solution, 16 mg of DMMB, 3.04 g of Glycine and 2.37 g of NaCl were dissolved in 800 ml of MilliQ. The solution was stirred vigorously and titrated to pH 3.0 with 0.1 M acetic acid. MilliQ was added up to a total volume of 1 L. The heparin standard solution was prepared by dissolving 5 mg of heparin in 1 ml of PBS. The solution was diluted, and volumes were pipetted into a 96-well plate correspondent to heparin concentrations from 0-5000 µg/ml. The samples were pipetted and stained with DMMB dye. The microplate was placed on a Clariostar Monochromator Microplate reader with 60 seconds of agitation before measurement of absorbance at 525 nm.

4.1.8. Heparin leaching test with DMMB

Four solutions in PBS of the following products were prepared: (1) pure fibrinogen (10.5 mg/ml), (2) fibrinogen (10.5 mg/ml) with non-conjugated heparin (6.75 mg/ml), (3) 50% modified (heparin-conjugated) fibrinogen, and (4) 75% modified (heparin-conjugated) fibrinogen. A volume of 100 µl of each solution was placed in a 48-well microplate in triplicate. The solutions were gently mixed with thrombin solution (10U/ml plus 5mM calcium chloride). Thereafter, the plate was incubated at

37ºC until gel formation. The gels were covered with 1 ml of PBS for hydration and kept in a 37ºC incubation. 1, 3 and 5 days after the gels preparation, 500 µl of the supernatant were collected per well and replaced with fresh buffer. On day 5, 200 µl of human plasmin (0.006 U per 200 µl volume of gel) were added to each gel and incubated overnight at 37ºC to induce gel degradation. A volume of 200 µl of sample and the same volume of DMMB dye solution were pipetted to a microplate, which was placed on a Clariostar Monochromator Microplate reader with 60 seconds of agitation before measurement of absorbance at 525 nm.

4.1.9. VEGF-A release profile based on ELISA

A VEGF-A in PBS solution was prepared with a concentration of 120 ng/ml. Three solutions in PBS were prepared: (1) pure fibrinogen (10.5 mg/ml), (2) 50% modified (heparin-conjugated) fibrinogen, and (3) 75% modified (heparin-conjugated) fibrinogen; and mixed with thrombin solution (10U/ml plus 5mM calcium chloride). The gels were prepared as previously described. Samples in triplicate were prepared in a microplate and in eppendorfs, and covered with 500 µl of buffer. A microplate was kept on 37ºC incubation in a static condition while eppendorfs were kept in a microplate shaker at 37ºC under agitation at a speed of 50 rpm. 1, 3, 5 and 7 days after the gels preparation, 500 µl of the buffer solution in each well were collected and replaced with fresh buffer. Each collected solution was stored at -20ºC. On day 10, 200 µl of human plasmin (0.006 U per 200 µl volume of gel) were added to each gel and incubated overnight at 37ºC. The next day, the degraded gels were collected and stored. For the analysis of the stored samples, the protocol of the VEGF-A Human ELISA kit (BMS277-2, ThermoFisher) was followed as described by the manufacturer.

4.1.10. Cell culture

Rat tenocytes were cultured in DMEM with low glucose (D6046, Sigma-Aldrich), containing 10% fetal bovine serum (FBS) and 1% penicillin-streptomycin (Pen/Strep), and maintained at an atmosphere of 5% CO_2, at 37 ºC. Medium was refreshed every 2 days. The cells were used when their confluency reached 80%-90% confluency.

4.1.11. Formation of HCF hydrogels and cell seeding

For the formation of HCF hydrogels, the previously described procedures were followed with the following conditions: 0%, 10%, 35% and 50% HCF; fibrinogen with non-conjugated heparin. 2D samples of cell suspension over coverslips were prepared in a 24-well microplate. 3D samples were prepared in a 96-well microplate, with the gels' solutions being mixed with cell culture. The seeding for both 2D and 3D samples was aimed for 2500 cells/cm^2. Cell culture medium was added to cover the gels.

4.1.12. Cell staining for fluorescence microscopy

Samples were fixed with 4% PFA for 30 m at RT, rinsed thoroughly with PBS and left hydrated until further use. Permeabilization was done with 0.1% Triton X-100 in PBS for 30min at RT, followed by a thorough PBS rinsing. Samples were stained with a 1:100 dilution of Alexa Fluor 568 Phalloidin (A12380, Thermo-Fisher) for 1h at RT, and counterstained with DAPI (0.2 µg/ml, Thermo-Fisher) in PBS for 10m at RT. Afterwards, the samples were washed with PBS and visualized with a Live Cell Nikon TI-E microscope.

4.2. Results

4.2.1. Nuclear Magnetic Resonance

From the NMR analysis, chemical shifts correspondent to NHS-Heparin and fibrinogen were revealed in the Heparin-conjugated fibrinogen sample (Fig. 13). Heparin's peaks (from approx. 2.5 to 3.5 ppm) and Fibrinogen's peaks (from approx. 1.75 to 2.5 ppm) are found in the modified fibrinogen NMR spectrum.

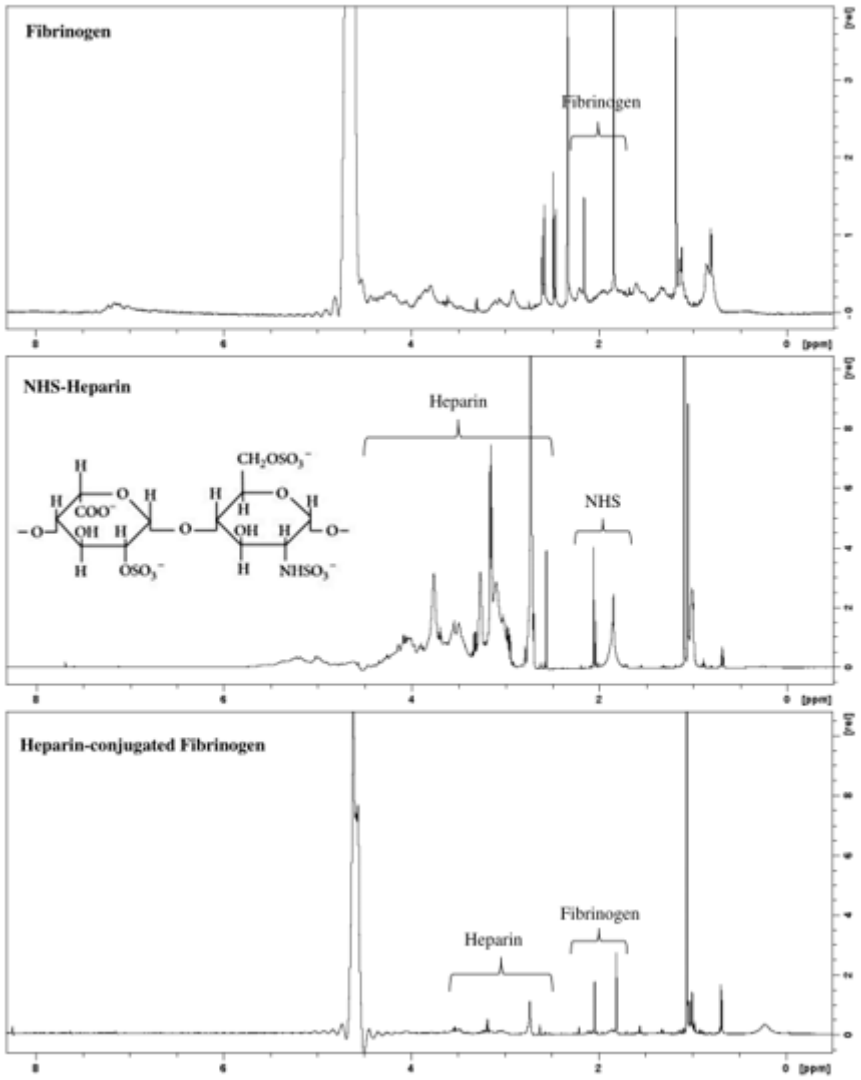

Fig. 13. NMR spectra of pure fibrinogen, NHS-heparin (activated heparin) and modified (heparin-conjugated) fibrinogen.

Tables 1 and 2 present the peaks of heparin and fibrinogen also identified in the modified fibrinogen NMR spectrum.

Table 1. Peaks in NMR spectra from pure fibrinogen and modified (heparin-conjugated) fibrinogen

Fibrinogen [ppm]	Modified Fibrinogen [ppm]
2.6074	2.6262
1.8474	1.8096

Table 2. Peaks in NMR spectra from between NHS-heparin (activated heparin) and modified (heparin-conjugated) fibrinogen

NHS-Heparin [ppm]	Modified Fibrinogen [ppm]
3.2653	3.223
3.1631	3.163
2.7872	2.7315
0.9962	0.9993

At least two peaks were found relevant (around the same ppm) and matched between the pure fibrinogen and the modified fibrinogen NMR spectra (Table 1). A higher number of matching peaks was found between the activated heparin and the modified fibrinogen NMR spectra. In this case, at least four matches were identified (Table 2).

4.2.2. Fourier-transform infrared spectroscopy

On the functional group region from the activated heparin spectrum, we can observe a N-H stretch around 3000 and 3400 cm^{-1}. The presence of noise can be observed between 3400 cm^{-1} and 4000 cm^{-1}, and 1300 cm^{-1} and 1800 cm^{-1}. Between 2300 cm^{-1} and 2400 cm^{-1}, the presented peak has a pattern that might be mistaken for one of the most common types of spectral artifacts in FTIR spectra, which is carbon dioxide. There are no significant peaks between 800 cm^{-1} and 1400 cm^{-1}. On the functional group region from the modified fibrinogen spectrum, we can observe an N-H stretch around 3000 and 3600 cm^{-1}. Again, the presence of noise can be observed between 1700 cm^{-1} and 2400 cm^{-1}.

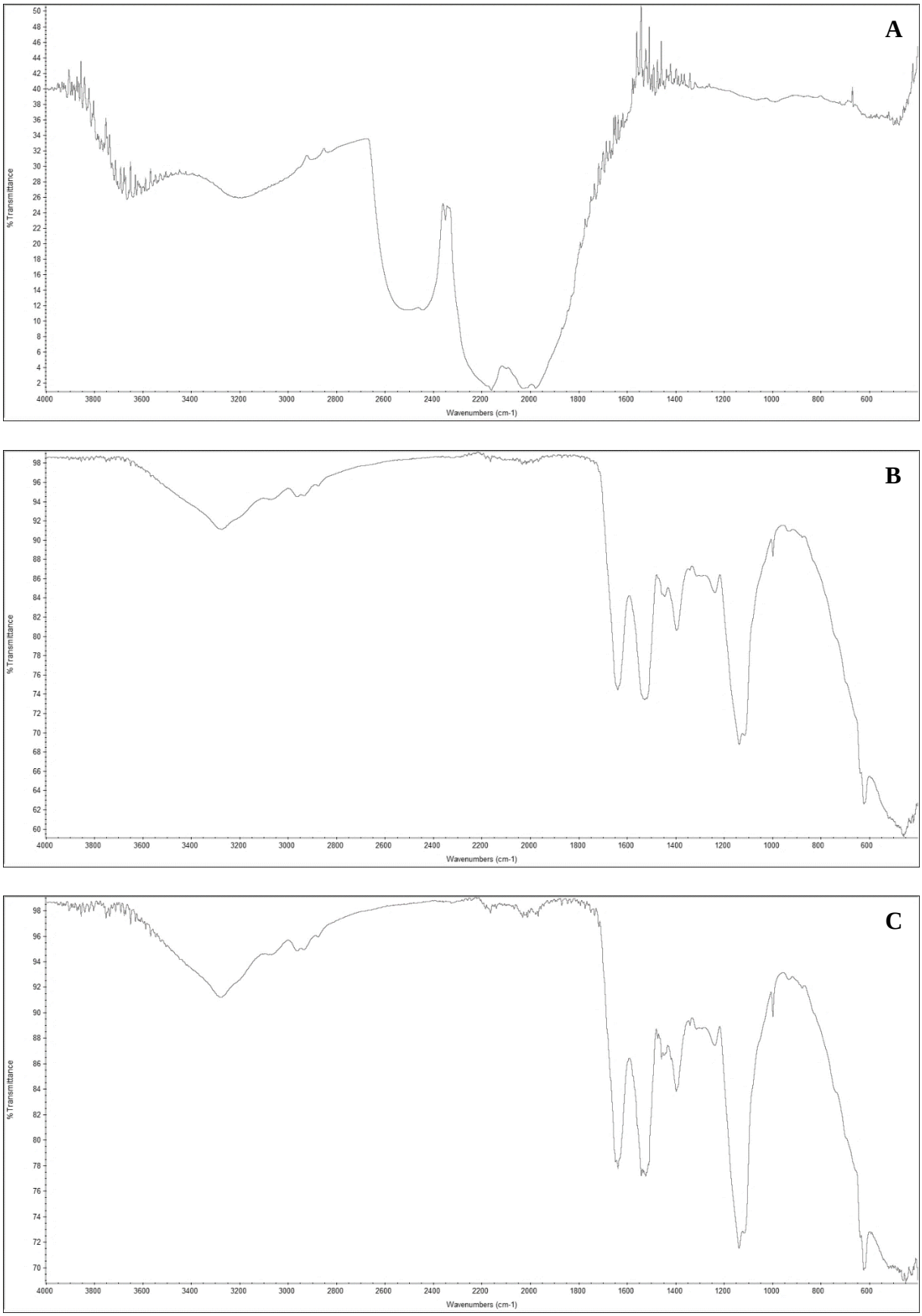

Fig. 14. FTIR transmission spectra of NHS-Heparin (activated heparin) (A), fibrinogen (B) and HCF (C).

It is not possible to observe any similarity between the FTIR spectra of the activated heparin and the HCF. However, the results demonstrate that there is a close similarity in the FTIR spectra pattern between pure fibrinogen and HCF (Figs. 14 and 15). There is a high correlation of peaks between the two spectra.

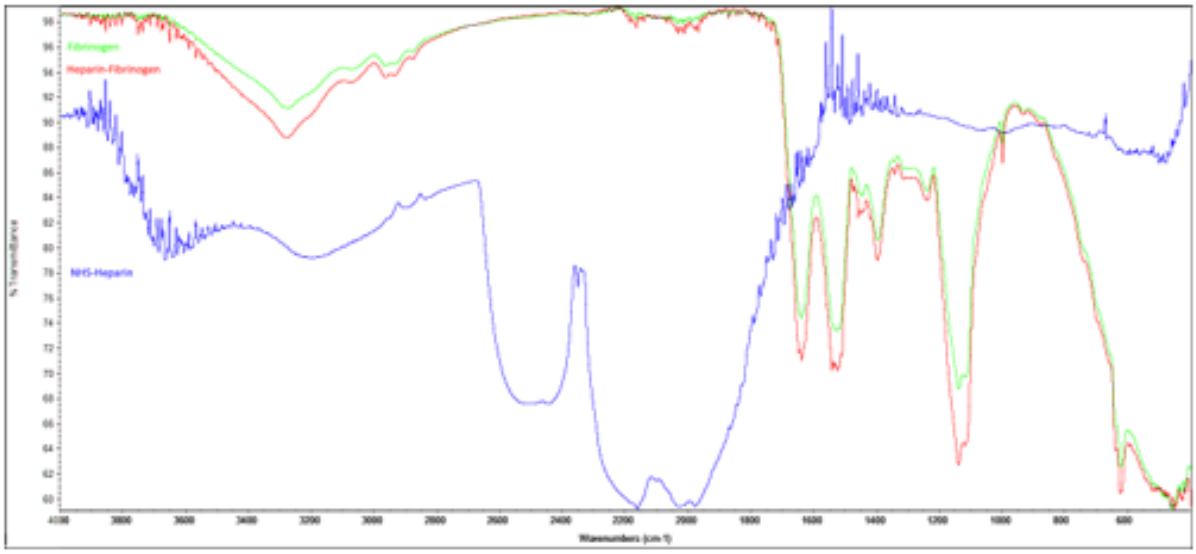

Fig. 15. FTIR transmission spectra of pure fibrinogen (in green), NHS-heparin (activated heparin) (in blue) and HCF (in red).

With a thorough analysis of the peaks, in the functional group region, between 3500 and 3700 cm^{-1}, an alcohol (O-H) group was identified as a match between the activated heparin and the modified fibrinogen FTIR spectra. The matching range is represented in blue (Fig. 16).

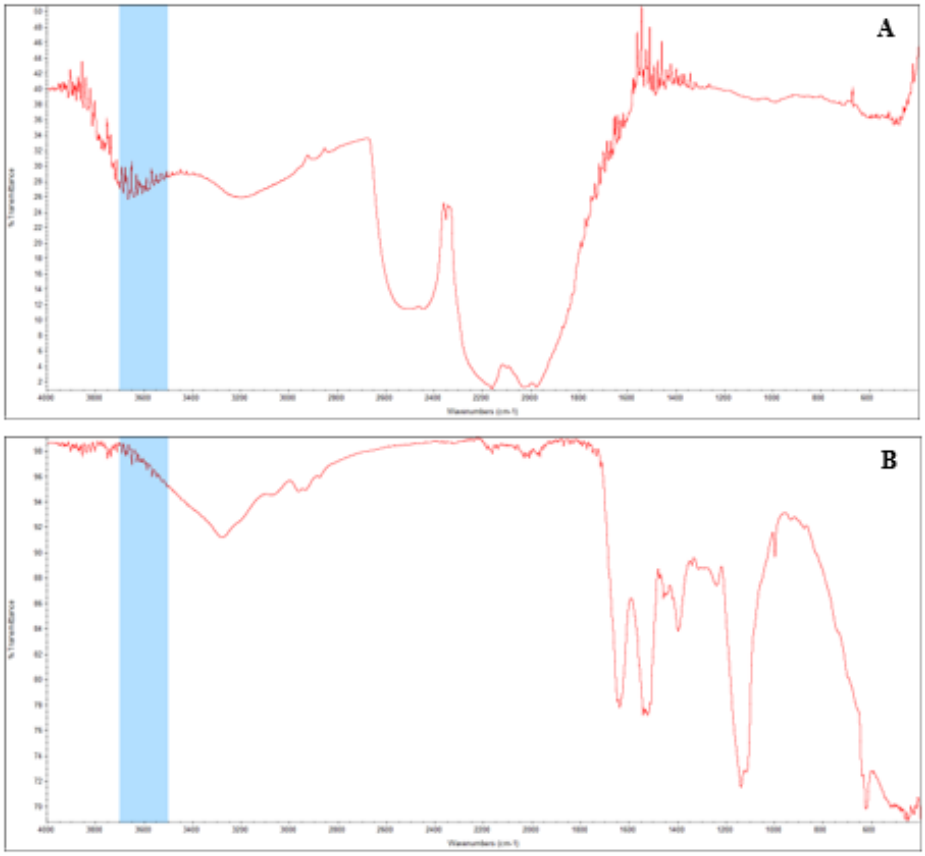

Fig. 16. FTIR transmission spectra of NHS-heparin (activated heparin) (A), and modified fibrinogen (B) with an alcohol (O-H) functional group range match (in blue).

4.2.3. Gelation kinetics and staining of matrices with alcian blue

For pure fibrinogen matrices, gelation took 15 minutes or less, while matrices with 40% and 50% of HCF took approximately 45 minutes to form. Solutions with 75% of HCF concentration took at least 1h to gelate, whereas 100% HCF matrices showed no signs of gelation.

Table 3. Gelation time of 0%, 40%, 50%, 75% and 100% modified (heparin-conjugated) fibrinogen matrices.

	Gelation time		
Percentage of HCF	***15 min***	***45 min***	***>60 min***
0%	✓		
40%		✓	
50%		✓	
75%			✓
100%			

The alcian blue stained matrices demonstrate the occurrence of phase separation. This can be noticed as the concentration of HCF increases and the color becomes more intense and saturated (Fig. 17 B, C and D).

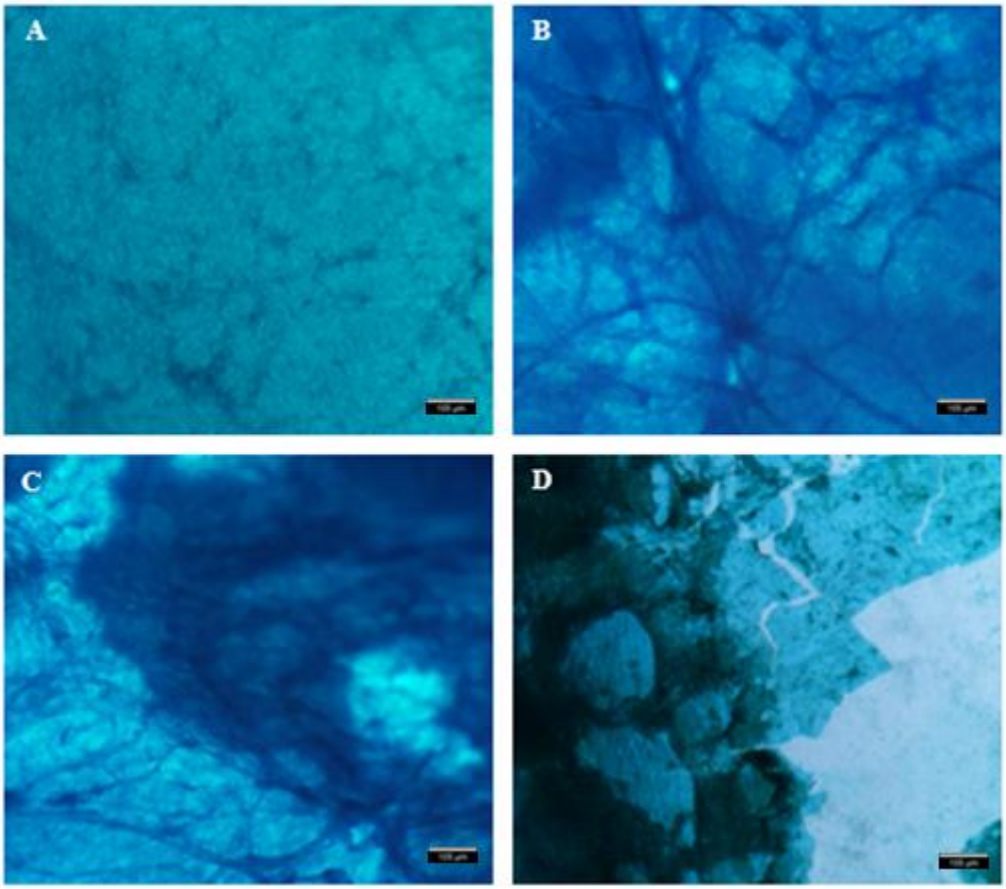

Fig. 17. Stained fibrinogen matrices with Alcian blue with 0% (A), 40% (B), 50% (C) and 75% (D) modified (heparin-conjugated).

4.2.4. Heparin quantification with 1,9-Dimethyl-Methylene Blue

The heparin quantification was performed to samples from three different conditions: (1) fibrinogen with non-conjugated heparin, (2) fibrinogen with conjugated heparin (before purification process), and (3) fibrinogen with conjugated heparin (after purification process). The DMMB assay's (Fig. 18) shows that the highest heparin concentration was observed in the fibrinogen with non-conjugated heparin sample, followed by the fibrinogen with conjugated heparin sample before the purification process. Fibrinogen with conjugated heparin after the purification process shows the lowest concentration of heparin.

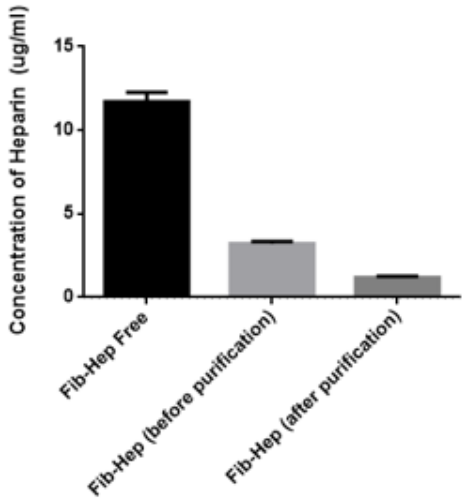

Fig. 18. Heparin concentration obtained from three different conditions: fibrinogen with non-conjugated heparin (Fib-Hep Free), fibrinogen with conjugated heparin (before purification process) and fibrinogen with conjugated heparin (after purification process).

4.2.5. Heparin leaching test with 1,9-Dimethyl-Methylene Blue

The heparin release from pure fibrin, HCF and fibrin with free heparin was quantified and compared over a 5-day period. As expected, pure fibrinogen samples showed an almost null and constant level at all timepoints. Fibrinogen with non-conjugated heparin showed a downward tendency, with about 4 μg/ml of heparin leached at day 1 and half of this value at day 2. A similar downward pattern was observed on 75% HCF sample, starting at day 1 with heparin leaching values between 6-8 μg/ml, reaching approximately 4 μg/ml at day 5. Lastly, regarding the 50% HCF sample, similar values of leached heparin were observed at day 1 and 5, between 4 and 5 μg/ml approximately, with a sudden peak at day 3 of about 7 μg/ml.

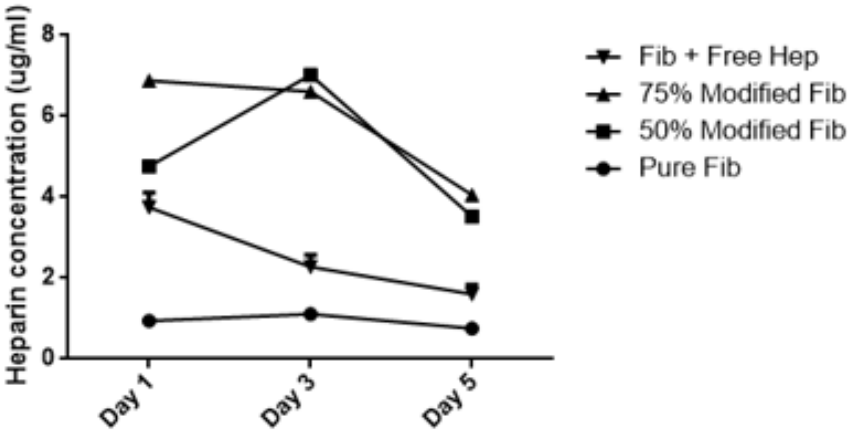

Fig. 19. Heparin leaching assay along days 1, 3 and 5 on four different conditions: pure fibrinogen, fibrinogen with non-conjugated heparin, 50 % and 75% HCF matrices

To evaluate the remaining concentration of heparin on the last day of the assay, the gels were degraded. Fibrinogen with non-conjugated heparin showed a lower heparin concentration in comparison to the 50% and 75% HCF samples (Fig. 20). In addition, the 75% HCF gels had a higher concentration of heparin in comparison to the 50% HCF gels. Pure fibrinogen gels presented residual values only.

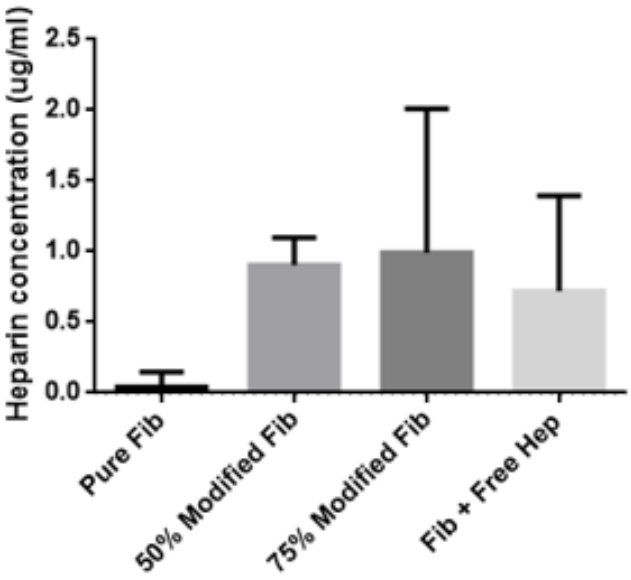

Fig. 20. Quantification of heparin retained in degraded gels (at day 5) on four different conditions: pure fibrinogen, fibrinogen with non-conjugated heparin, 50 % and 75% HCF matrices

4.2.6. VEGF-A release profile

The VEGF-A release profile was performed with pure fibrinogen, fibrinogen with non-conjugated heparin and HCF samples, with a duration of 7 days in static and non-static incubation conditions.

In static conditions (Fig. 21), an upward movement was observed in all the samples. Pure fibrinogen and HCF samples presented a similar behavior until day 5, where pure fibrinogen's release values began to rise. HCF matrices showed the lowest VEGF-A release value at day 7.

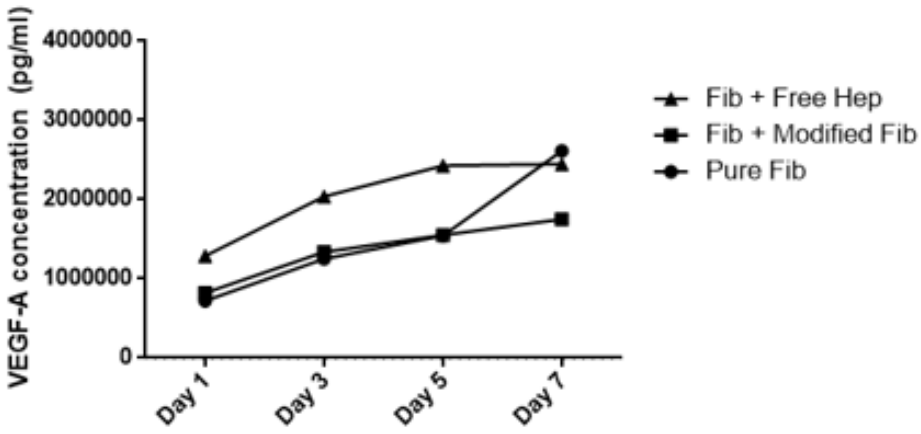

Fig. 21. VEGF-A Release Profile without agitation (days 1, 3, 5 and 7) on three different conditions: pure fibrinogen, fibrinogen with non-conjugated heparin and HCF matrices

For dynamic conditions (Fig. 22), all showed a stabilized behavior with VEGF-A released concentrations under 500 ng/ml, except fibrinogen with non-conjugated heparin matrices that showed a sudden increase of the VEGF-A release values up to approximately 200 ng/ml at the last day of the assay.

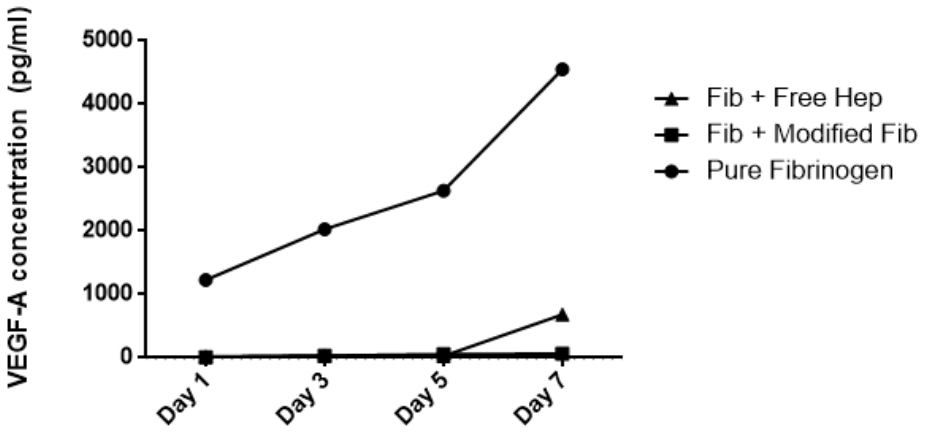

Fig. 22. VEGF-A Release Profile with agitation (days 1, 3, 5 and 7) on three different conditions: pure fibrinogen, fibrinogen with non-conjugated heparin and HCF matrices

The results from the quantification of VEGF-A on gels degraded in day 10 show that pure fibrin hydrogels retain more VEGF-A in both with and without agitation conditions (Fig. 23). HCF matrices showed to retain less VEGF-A in both conditions at the last day of the assay.

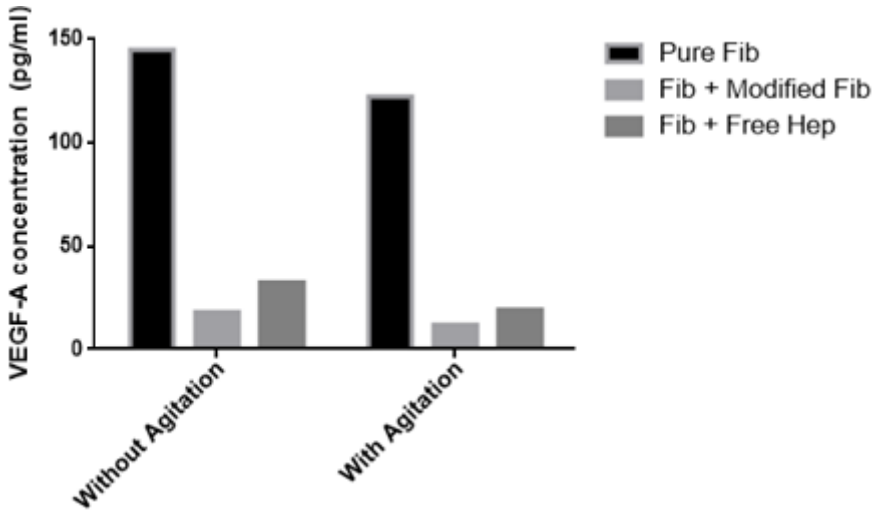

Fig. 23. VEGF-A retained in degraded gels with and without agitation (day 10) on three different conditions: pure fibrinogen, fibrinogen with non-conjugated heparin and HCF matrices

4.2.7. Cell attachment study

The fluorescent images demonstrate the morphology of the cells on the different HCF's concentrations matrices upon fixation (Fig. 24). In the Bright-field image, it is presented the control used to observe the morphology of live tenocytes in 2D (Fig. 24 A).

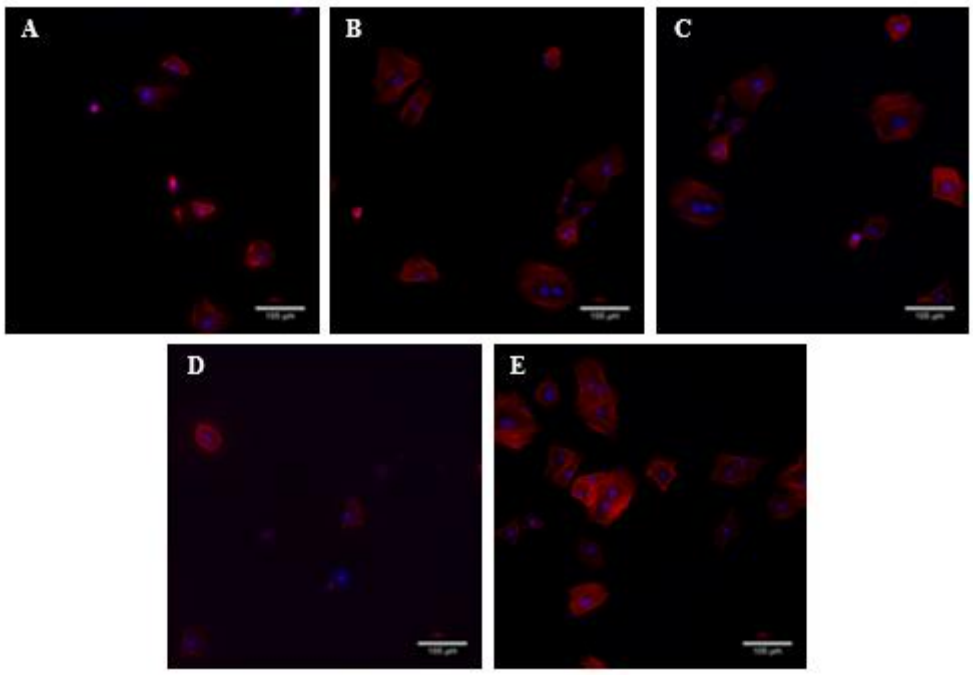

Fig. 24. Fluorescent images of 3D hydrogel samples embedded with rat tenocytes and stained with Phalloidin (red), and counterstained nuclei with DAPI (blue): 0% (A), 10% (B), 35% (C), 50% modified (heparin-conjugated) fibrinogen hydrogel (D), and fibrinogen with non-conjugated heparin (E). The scalebar represents 100 µm.

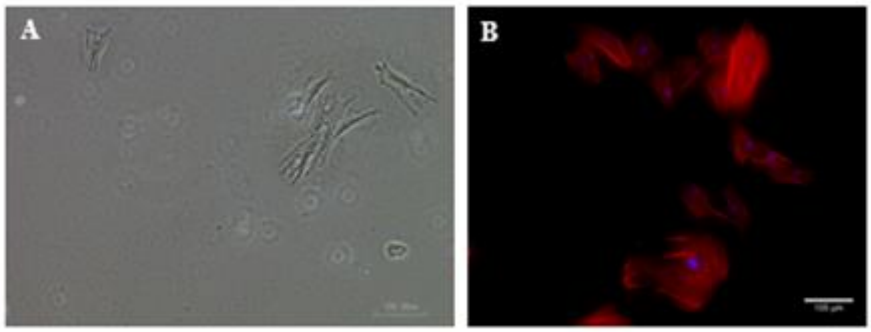

Fig. 25. Bright-field image of tenocytes cultured on 2D (day 1 of culture) (A) and fluorescent image of tenocytes stained with Phalloidin and DAPI (B). The scalebar represents 100 µm.

Tenocytes with a spread/elongated morphology were found in all HCF hydrogel samples. The imaging was performed in random regions of the samples.

4.3. Discussion

NMR spectra analysis

It should be noted that it was not mentioned, in the section 4.1.2, the first procedure created for the synthesis of Heparin-conjugated Fibrinogen (Appendix 1). The first procedure corresponds to a first attempt in the initial stage of the experimental activity to obtain the modified fibrinogen product, which was inspired by M. Kim *et al.* (2014) and H. Yang *et al.* (2010). Later on, the procedure was re-designed since the activation of heparin (12h) and reaction time with fibrinogen (3h) were found to be extensive and have a negative effect on the stability of reagents that are readily hydrolyzed. The steps were simplified, and the reaction's concentrations, pH and temperature were adjusted. The first trial of synthesis of modified fibrinogen product was analyzed by NMR (Appendix 3). At first, the purpose was to recognize fibrinogen in the spectrum mainly by its characteristic sodium citrate peak. However, it was observed that this peak did not appear in the NMR spectra, probably due to the purification process involving dialysis. To check this hypothesis, a second NMR spectroscopic analysis was conducted with a non-dialyzed modified fibrinogen, which in fact presented the sodium citrate peak, highlighting the effect of dialysis in the elimination of this compound.

As seen in Fig. 13, the chemical shifts of activated heparin were found to correlate with the ones presented by the HCF. In addition, it was also possible to identify matching peaks from heparin in the modified fibrinogen samples (Tables 1 and 2). A list of matching peaks between two or more substances was generated based on the ppm band range and the intensity of the signals. In that way, if two peaks or more peaks are found in a near ppm location and show similarities in signal intensity, the peaks are matched and retrieved. Chemical shifts correspondent to NHS-Heparin and fibrinogen were revealed in the HCF sample (Fig. 13). In a study based on the ^{1}H-NMR spectra of 31 pure heparins, chemical shifts for peaks in heparin were always present at 5.42, 5.23, 5.01, 4.82, 4.60, 4.40, 4.34, 4.27, 4.12, 4.03, 3.87, 3.77, 3.67, 3.40, 3.28, and 2.05 ppm. A correlation with the ^{1}H-NMR HCF spectrum is found, where the relative intensities of the previously mentioned peaks vary, however, the chemical shifts differ only by <0.03 ppm (Z. Zhang et al., 2009). As expected, the N-acetyl protons of heparin show a single peak at 2.04 ppm (± 0.02ppm). A small dermatan sulfate peak, corresponding to N-acetyl protons of dermatan sulfate, shows near 2.08 ppm (The Federal Institute for Drugs and Medical Devices (BfArM), 2017). With this, we can conclude that there was heparin in the product subjected to analysis. However, it is inconclusive if that heparin is free or is conjugated to fibrinogen.

FTIR spectra analysis

For FTIR spectral reliability purposes, the spectra of sample and from the background were obtained at least twice. In this way, there were less chances of the presence of peaks not caused by the sample and, in general, due to FTIR spectral artifacts. Hence, the peak found with a similar pattern to carbon dioxide was not considered as so.

FTIR spectra has two general regions (Fig. 14-16): the functional group region, which is between 1500 and 4000 cm^{-1}; and the fingerprinting region, which is between 400 and 1500 cm^{-1}.

According to the results, the N-H stretch found in the spectrum of modified fibrinogen corresponds to the fibrinogen's N-H stretch. It was possible to relate the matching peaks revealed with NMR spectra with the peaks found in the FTIR spectrum, by conjugating the information of signal intensity and range of signal reveal. With this information, an alcohol (O-H) group from heparin was found in common with the modified fibrinogen, in a range between 3550-3700 cm^{-1} (Fig. 16).

Gelation kinetics and alcian blue staining

Regarding the gelation time, it was observed that it increases as the modified fibrinogen concentration in the hydrogels increases. In opposition, the lower the concentration of modified fibrinogen, the shorter was the time of gelation.

Staining with alcian blue enabled a gross observation of heparin present within the hydrogels, since this dye forms salt linkages with the acid groups of sulfated glycosaminoglycans. Ideally, the hydrogels should be uniformly composed of modified fibrinogen, thus yielding a homogenous blue tonality throughout the whole sample. However, as the concentration of modified fibrinogen increased, the hydrogels' staining color intensified and it was easier to observe phase separation; whereas the hydrogels formed with pure fibrinogen showed a consistent and uniform polymerization. Phase separation is a macroscopic phenomenon which is only observed when the size of the aggregates allows light scattering. Fibrinogen is a large molecule and its dimension might facilitate the observation of this phenomenon even in pure solution conditions (Fig. 17 A). In terms of modified fibrinogen gel conditions (Fig. 17 B, C and D), this behavior could be explained by the crosslinking of fibrinogen with heparin and increased dimensions of the molecular structure, as well as the non-addition of fibrin stabilizer factors such as factor XIII.

Heparin quantification

With these results, we may conclude the presence of heparin in the HCF product, as well as the removal of non-conjugated heparin during dialysis. This last fact is confirmed due to HCF samples obtained after dialysis presenting the lowest concentration of heparin.

Heparin leaching assay

It was expected that pure fibrinogen samples would present zero heparin concentration. However, even though DMMB assay is widely accepted for its specific measurement of sulfated GAGs, due to fibrinogen's properties and interaction with DMMB dye, residual values were detected. At day 1, 50% and 75% HCF samples presented a non-expected behavior by showing higher values of leached heparin in comparison to non-conjugated gel samples. In addition, the highest amount of leached heparin at day 1 was presented by the 75% HCF gel samples. However, this fact might be justified by the possibility of the collected buffer from day 1 to contain non-retained heparin residues. Throughout the experiment, it is possible to observe a decrease of the amount of leached heparin by 75% HCF gels because of the recurrent buffer changes. On day 3 and day 5, the values of leached heparin decrease to similar values presented by 50% HCF samples. These results might be translated in signals of saturation at 50% HCF, i.e. gels formed with a percentage higher than 50% will not retain heparin. The same pattern is found in fibrinogen with non-conjugated heparin samples, with the highest value of heparin leaching during the assay's time-period also being presented at day 1 and a consistent decrease behavior until day 5. For the 50% HCF gels, there is the appearance of a sudden peak at day 3. However, the pattern changes and begins to show the expected decreasing behavior. In addition, the quantification of retained heparin in degraded matrices at the last day of the assay was also performed, pointing out 75% HCF matrices as the ones retaining more heparin, in comparison to pure fibrinogen, 50% HCF and fibrinogen with non-conjugated heparin samples (Fig. 20). With these results, it is possible to confirm the attachment of heparin in HCF gels with a saturation level of 50%.

VEGF-A release profile

During a period of 7 days, modified fibrin matrices showed the lowest VEGF-A release in static conditions, in comparison to pure fibrinogen and fibrinogen with non-conjugated heparin matrices. In non-static conditions, the release of the growth factor remained constant and under 500 ng/ml. This concentration value is considered low and not significant since residual growth factor release from hydrogels is unavoidable. Hence, these results points to the ability of modified fibrin matrices in retaining VEGF-A.

Cell attachment in modified fibrin hydrogels

The aim of this assay was to find out if the matrices formed with HCF were able to support cells attachment and spreading. According to Kalson *et. al* (2015), mouse tendon cells in 2D cell culture have a flat shape and a characteristic appearance of fibroblasts (Fig. 26).

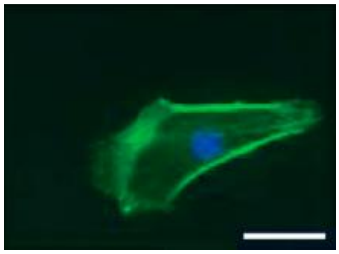

Fig. 26. Shape of isolated mouse tendon cell from E15.5 in 2D culture. The scalebar represents 10 µm. Adapted from (Kalson *et al.*, 2015).

2D samples with cell suspensions over coverslips were used as a control to determine the cells morphology and for further comparison purposes. It was observed that cells in a necrotic state presented a round shape, whereas live cells presented a spread elongated shape. In all the 3D HCF samples, cells with similar morphologies were found. However, conclusions about cell adhesion, spread and growth abilities in the different HCF gel conditions were not made because of the observed phase separation on the alcian blue stained gels, which could have compromised the cell seeded surface and environment.

Chapter 5: Fabrication of electrospun pNIPAM microfibers

5.1. Materials and Methods

5.1.1. Preparation of polymer solution

The solutions for electrospinning were prepared by dissolving pNIPAM in a solvent mixture of chloroform and DMF with a volume ratio of 3:1 and 7:3, at a concentration of 40% and 50% (w/v), respectively. The solutions were mixed overnight with a stir bar and immediately used in the next day.

5.1.2. Electrospun fibers formation and imaging

The environmental conditions were kept constant with temperature at 23ºC and humidity at 28%. The solutions were loaded into 5 mL plastic syringes and fed to the needle tip using a syringe pump. Positive voltages of 10, 20 and 25 kV were applied to the needle using a high voltage power supply. Respectively, the collector was placed at distances of 11.6, 10 and 13 cm from the needle tip. On applying high voltage, the polymer solution formed a Taylor cone at the needle tip and a positively charged jet was sprayed on a rotating mandrel collector at maximum speed. The electrospun fibers were collected on aluminum plates. The fibers were sputter-coated with gold, and their morphology was observed and recorded with a Nikon SMZ25 Stereomicroscope and a FEI/Philips XL30 Scanning Electron Microscope.

5.2. Results

All the electrospun fiber samples obtained from the different conditions presented a reasonable alignment and parallel pattern. This aspect was more notable in the 40% pNIPAM in a 7:3 chloroform/DMF ratio sample, however, overlapping was observed and the bottom layer of the fibers was found weak (Fig. 27).

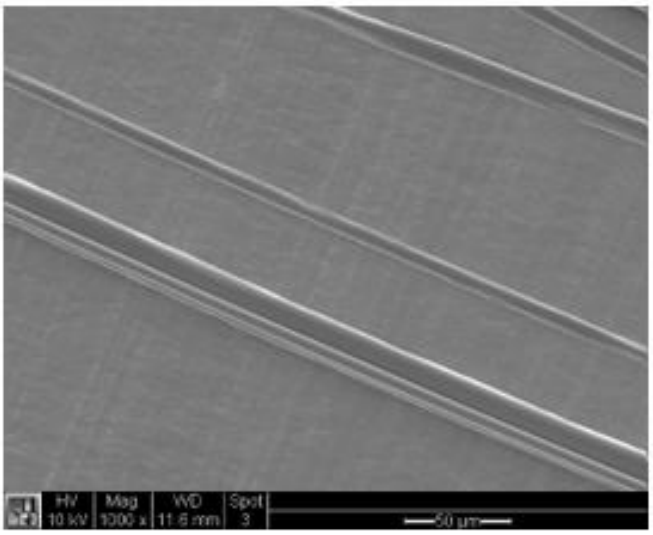

Fig. 27. Scanning electron microscopy image of a 40% pNIPAM electrospinning sample with 2.5 ml/h of flow rate, 10 kV of voltage and 11.6 cm of working distance (WD) in 7:3 Chloroform/DMF ratio. The scalebar represents 50 µm.

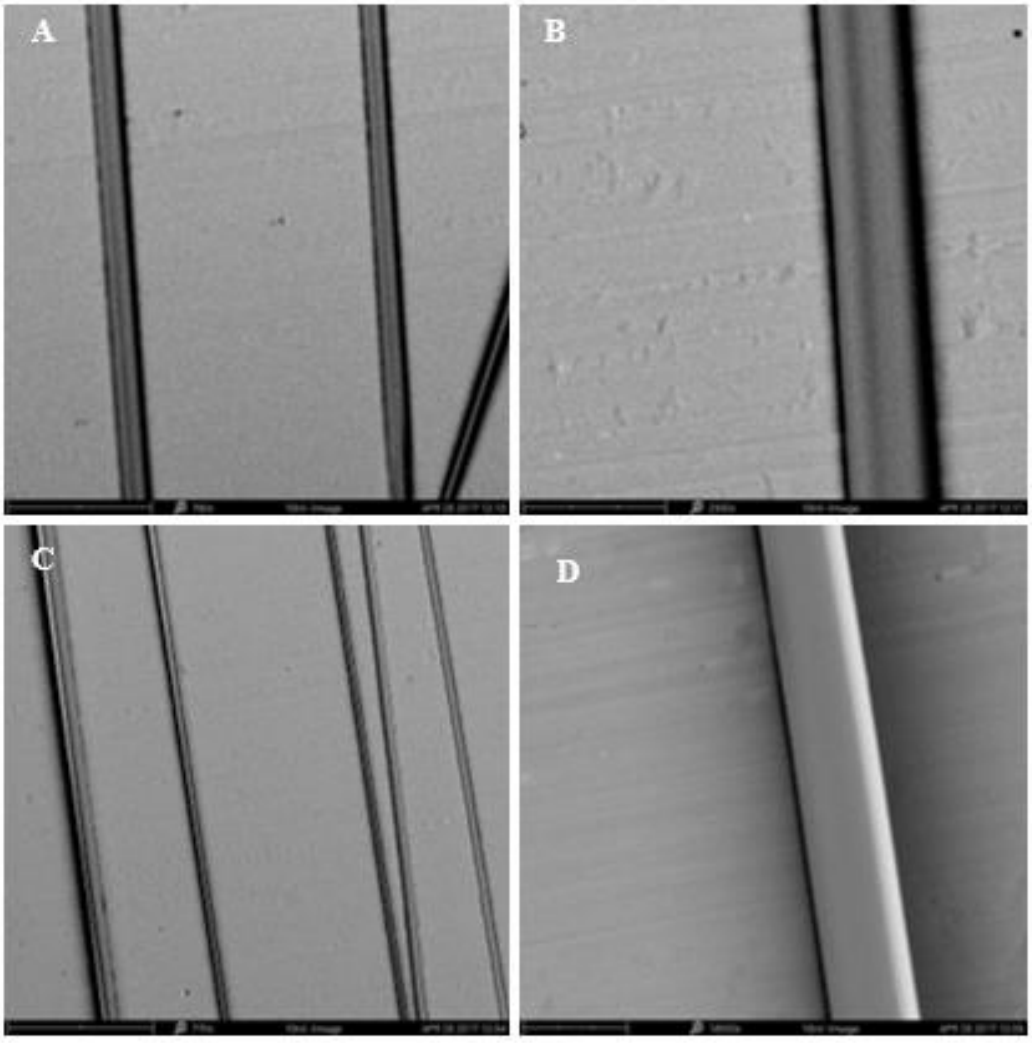

Fig. 28. Scanning electron microscopy image of 50% pNIPAM electrospinning samples in 7:3 Chloroform/DMF ratio. Two images of a sample (A and B) with 2.5 ml/h of flow rate, 25 kV of voltage and 13 cm of working distance (WD). And, two images of a sample (C and D) with 2.5 ml/h of flow rate, 20 kV of voltage and 10 cm of WD. The scalebar represents 100 (A), 20 (B), 50 (C) and 10 µm (D).

Fibers from 50% pNIPAM in a 7:3 chloroform/DMF ratio presented a flattened aspect which affected their cylindrical shape (Fig. 28).

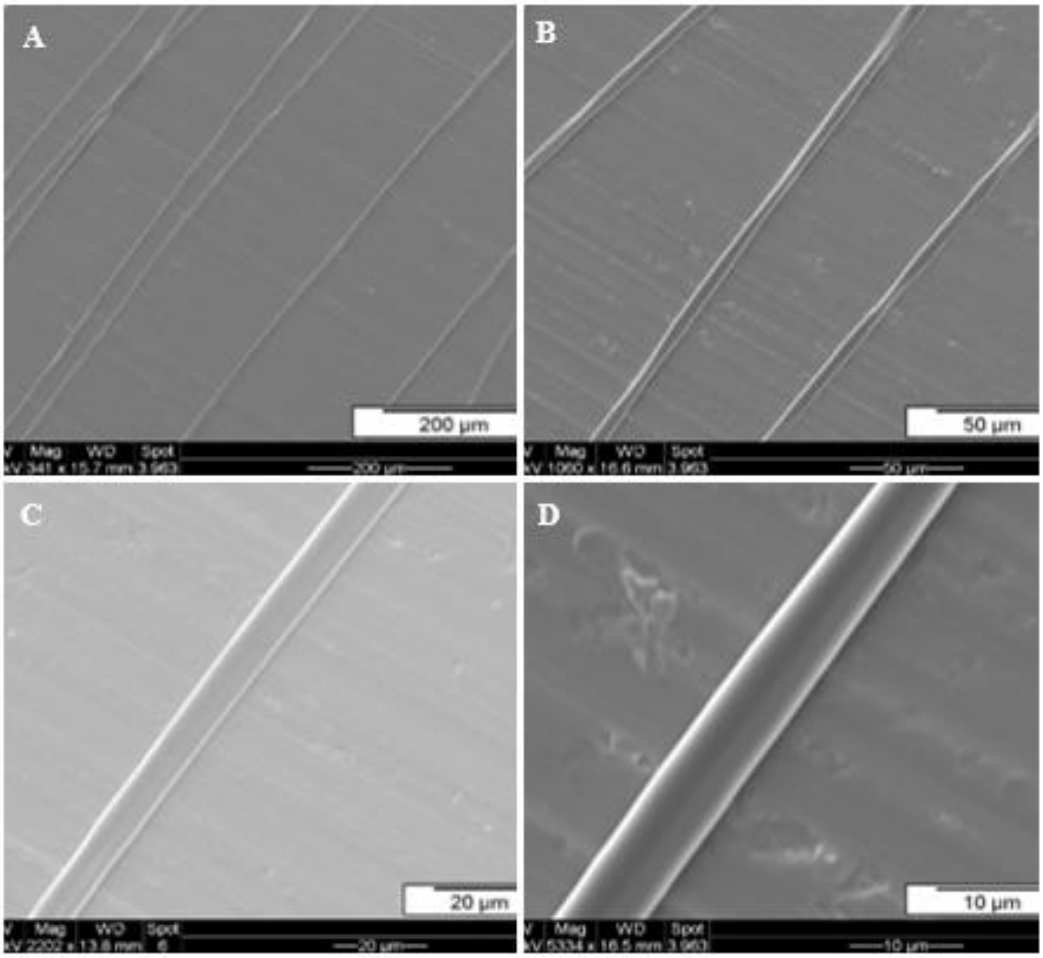

Fig. 29. Scanning electron microscopy images of a 40% pNIPAM electrospinning sample in 3:1 Chloroform/DMF ratio. The scalebar represents 200 (A), 50 (B), 20 (C) and 10 µm (D).

Similarly, some of the electrospun fibers from 40% pNIPAM in a 3:1 chloroform/DMF ratio sample also presented an irregular tubular morphology with some narrowed regions along the fibers (Fig. 29).

5.3. Discussion

The fibers that most suited the desired properties - tubular appearance, diameter between 5-20 µm (for resemblance of vessels' diameter range *in vivo*) and a linear and parallel alignment (for cells orientation) - were found to be obtained from 40% pNIPAM in a 3:1 chloroform/DMF ratio. Even though some fibers did not seem to consistently present a cylindrical/tubular appearance over the sample surface (Fig. 29 A and B), and narrowed regions were found along some of the fibers, most of them did not present this aspect and were considered reasonable (Fig. 29 C and D).

Electrospun fibers from 40% pNIPAM in a 7:3 chloroform/DMF ratio presented notable characteristics of alignment and parallel pattern but the overlapping and bottom layer weakness of the fibers were found to be a concern (Fig. 27).

Finally, from 50% pNIPAM in a 7:3 chloroform/DMF ratio, in comparison to the other samples, the resulting fibers were found reasonable, even though a flattened aspect presented in the surface was observed (Fig. 28 B and D).

Chapter 6: Conclusion

TE is a multidisciplinary area, thus in order to obtain functional products with quality, the cooperation between the various disciplines that comprise it must remain active and dynamic. An accurate understanding of biomaterials and cell biology with emphasis on cell differentiation, cell interaction and extracellular matrix formation is of great importance to succeed in tissue regeneration. It is also important to highlight the importance of dealing with and overcoming the emerging obstacles originated by the community related to cell seeding ethics.

TE has a high market potential, hence investment in this area has grown in a gradual and sustained manner. Despite of this, the industry linked to the production of biomimetic 3D models still faces numerous challenges to improve the characteristics of the models and ensure the improvement of their performance.

This thesis work can be divided into three main stages which involved:

1. the process of optimizing and characterizing the hydrogel;
2. seeding with tenocytes in order to test cell behaviors in the hydrogel, and
3. fabricating pNIPAM microfibers for the hydrogel microchanneling.

It was possible to optimize the production process of the hydrogel that resulted in the activation of heparin and its binding to fibrinogen, as observed through NMR and FTIR spectroscopic analysis. In relation to gelation time tracking, it was observed that as the HCF concentration increased, the time of gelation of the hydrogels increased as well. The staining of hydrogels with alcian blue pointed to some polymerization issues with 40%, 50% and 75% HCF. In spite of that, the hydrogels demonstrated the capacity to covalently attach heparin with a saturation limit of 50% HCF, and retain VEGF-A, as observed with hydrogels staining with dimethylmethylene blue and ELISA analysis. It was also successfully confirmed and identified the morphology of tenocytes in 3D HCF hydrogels. However, conclusions about adhesion, spreading and growth abilities in the different HCF gel conditions were made because of the observed phase separation on the alcian blue stained gels, which could have compromised the cell seeded surface and environment. Finally, it was observed that electrospun fibers obtained from 50% pNIPAM in a 7:3 chloroform/DMF ratio and 40% pNIPAM in a 3:1 chloroform/DMF ratio enabled to obtain the desired fiber diameter (5-20 μm) and alignment (linear and parallel).

In terms of limitations, a large amount of time was devoted to the analysis of NMR and FTIR spectra. The problem in NMR and IR spectroscopy is that the more complex the composition of a sample, the more difficult it becomes to understand what peaks correspond to functional groups, and to recognize its characteristic signals. Characterization assays of the HCF hydrogels were often delayed because not

enough HCF product was being obtained after each prepared batch - final amount of product obtained from the entire hydrogel fabrication process, since the first step of activation of heparin to the last step of freeze-drying. Several attempts were conducted in order to obtain proper electrospun fibers samples. These attempts regard the complexity of obtaining proper and consistent fibers without having already determined machine configurations and a "recipe" to prepare the polymer solution, in order to achieve the desired results. In specific, the most recurrent issue during the electrospinning procedure was the splitting of the Taylor Cone, which returned from none to just a few non-aligned fibers under the expected diameter range. Assays towards achieving microchanneling in the hydrogels were not performed because a reasonable amount of results regarding the optimized properties of the hydrogel were expected before the embedding of the fibers.

In terms of future perspectives, it is suggested a continued optimization of the HCF hydrogels' formation process in order to improve the acquisition of a consistent HCF product in larger amounts, consequently avoiding the need of constant batch preparation and delay of important and further investigation assays. In addition, the formation of HCF hydrogels should be studied in variations of solution pH, temperature, fibrinogen and thrombin concentrations, addition of stabilizers and anti-degradation factors, in order to minimize polymerization difficulties. These might have been caused by the fibrinogen concentration (as shown by the results, pure fibrinogen concentration has a high influence in the gelation and polymerization process), the thrombin and calcium chloride concentrations (whose unreasonable mixed ratios may result in a less stable fibrin gel), and/or the non-addition of crosslinkers to matrix formula (factor XIII and others are usually used in gel formation because of their positive effect and enhancement of the formation of a homogeneous and complex polymerized network), among others. It is also suggested a better characterization of the hydrogels, especially in situations of cells incorporation, to determine with certainty the effect of the fabricated 3D environment in cell behavior. In the future, it is intended to achieve a better usage of the 3D biomimetic models' potential for the repair and regeneration of tissues, as well as the understanding and cure of pathologies; as in specific, the results obtained are expected to contribute to the development of neuronal and vascular biomimetic models, either singular or combined, for in vitro studies and regenerative applications.

Bibliography

Australian Centre for Microscopy & Microanalysis (AMMRF). (2013). SEM Layout | MyScope. Retrieved August, 2017, from http://www.ammrf.org.au/myscope/sem/practice/principles/layout.php

Badami, V., & Ahuja, B. (2014). Biosmart materials: breaking new ground in dentistry. *The Scientific World Journal*, *2014*, 986912. https://doi.org/10.1155/2014/986912

Baker, M. J., Trevisan, J., Bassan, P., Bhargava, R., Butler, H. J., Dorling, K. M., … Martin, F. L. (2014). Using Fourier transform IR spectroscopy to analyze biological materials. *Nature Protocols*, *9*(8), 1771–91. https://doi.org/10.1038/nprot.2014.110

Battler, Alexander, Leor, J. (2007). *Stem Cell and Gene-Based Therapy: Frontiers in Regenerative Medicine - Google Livros*. New York: Springer.

Biazar, E., Khorasani, M. T., Montazeri, N., Pourshamsian, K., Daliri, M., Rezaei, M., … Roviemiab, Z. (2010). Types of neural guides and using nanotechnology for peripheral nerve reconstruction. *International Journal of Nanomedicine*, *5*, 839–52. https://doi.org/10.2147/IJN.S11883

Bio-Rad. (2017a). ELISA Procedure. Retrieved August, 2017, from https://www.bio-rad-antibodies.com/elisa-procedure.html

Bio-Rad. (2017b). Types of ELISA. Retrieved August, 2017, from https://www.bio-rad-antibodies.com/elisa-types-direct-indirect-sandwich-competition-elisa-formats.html#Sandwich

Bruker Optics. (2012). ATR: Advantages for FT-IR Spectroscopy. Retrieved August, 2017, from https://www.azom.com/article.aspx?ArticleID=5958

C.K.S., Pillai, Willi, Paul, Chandra P., S. (2009). Chitin and chitosan polymers: Chemistry, solubility and fiber formation. *Progress in Polymer Science*, *34*(7), 641–678. https://doi.org/10.1016/J.PROGPOLYMSCI.2009.04.001

Chaurey, V., Block, F., Su, Y.-H., Chiang, P.-C., Botchwey, E., Chou, C.-F., & Swami, N. S. (2012). Nanofiber size-dependent sensitivity of fibroblast directionality to the methodology for scaffold alignment. *Acta Biomaterialia*, *8*(11), 3982–3990. https://doi.org/10.1016/j.actbio.2012.06.041

Chen, Qizhi, Liang, S., & A. Thouasb, G. (2013). Elastomeric biomaterials for tissue engineering. *Progress in Polymer Science*, *38*(3–4), 584–671. https://doi.org/10.1016/J.PROGPOLYMSCI.2012.05.003

Chen, C., Tang, Y., Vlahovic, B., & Yan, F. (2017). Electrospun Polymer Nanofibers Decorated with Noble Metal Nanoparticles for Chemical Sensing. *Nanoscale Research Letters*, *12*(1), 451. https://doi.org/10.1186/s11671-017-2216-4

Chen, T. S. N., Peter, M., & Chen, S. Y. (1994). The myth of Prometheus and the liver. *Journal of the Royal Society of Medicine*, *87*. Retrieved from https://www.ncbi.nlm.nih.gov/pmc/articles/PMC1294986/pdf/jrsocmed00078-0036.pdf

Chou, S.-F., Carson, D., & Woodrow, K. A. (2015). Current strategies for sustaining drug release from electrospun nanofibers. *Journal of Controlled Release : Official Journal of the Controlled Release Society*, *220*(Pt B), 584–91. https://doi.org/10.1016/j.jconrel.2015.09.008

Conolly W. Bruce, Benanzio, M. (2007). Hand Transplantation. *Springer*.

Dahlin, C., Johansson, A., Hoffman, M., & Molenberg, A. (2014). Early biocompatibility of poly (ethylene glycol) hydrogel barrier materials for guided bone regeneration. An *in vitro* study using human gingival fibroblasts (HGF-1). *Clinical Oral Implants Research*, *25*(1), 16–20. https://doi.org/10.1111/clr.12076

Dahlmann, J., Krause, A., Möller, L., Kensah, G., Möwes, M., Diekmann, A., … Dräger, G. (2013). Fully defined in situ cross-linkable alginate and hyaluronic acid hydrogels for myocardial tissue engineering. *Biomaterials*, *34*(4), 940–951. https://doi.org/10.1016/j.biomaterials.2012.10.008

Dreyfuss JL, Regatieri CV, Jarrouge TR, Cavalheiro RP, Sampaio LO, Nader HB. Heparan sulfate proteoglycans: structure, protein interactions and cell signaling. *An Acad Bras Cienc.* 2009 Sep;81(3):409-29. Review. PubMed PMID: 19722012. Retrieved from: https://www.ncbi.nlm.nih.gov/pubmed/19722012

Dvorak, H. F., Brown, L. F., Detmar, M., & Dvorak, A. M. (1995). Vascular permeability factor/vascular endothelial growth factor, microvascular hyperpermeability, and angiogenesis. *The American Journal of Pathology*, *146*(5), 1029–39. Retrieved from http://www.ncbi.nlm.nih.gov/pubmed/7538264

Elahi, M. F., Guan, G., Wang, L., & King, M. W. (2014). Influence of layer-by-layer polyelectrolyte deposition and EDC/NHS activated heparin immobilization onto silk fibroin fabric. *Materials*, *7*(4), 2956–2977. https://doi.org/10.3390/ma7042956

Félix Lanao, R. P., Jonker, A. M., Wolke, J. G. C., Jansen, J. A., van Hest, J. C. M., & Leeuwenburgh, S. C. G. (2013). Physicochemical properties and applications of poly(lactic-co-glycolic acid) for use in bone regeneration. *Tissue Engineering. Part B, Reviews*, *19*(4), 380–90. https://doi.org/10.1089/ten.TEB.2012.0443

Gelse, K., Pöschl, E., & Aigner, T. (2003). Collagens--structure, function, and biosynthesis. *Advanced Drug Delivery Reviews*, *55*(12), 1531–46. Retrieved from http://www.ncbi.nlm.nih.gov/pubmed/14623400

Hobson, M. I., Green, C. J., & Terenghi, G. (2000). VEGF enhances intraneural angiogenesis and improves nerve regeneration after axotomy. *Journal of Anatomy*, *197 Pt 4*(Pt 4), 591–605. https://doi.org/10.1046/J.1469-7580.2000.19740591.X

Höflinger, G. (2013, August). Brief Introduction to Coating Technology for Electron Microscopy. Retrieved from http://www.leica-microsystems.com/science-lab/brief-introduction-to-coating-technology-for-electron-microscopy/

Huang, C., Ouyang, Y., Niu, H., He, N., Ke, Q., Jin, X., … Lin, T. (2015). Nerve Guidance Conduits from Aligned Nanofibers: Improvement of Nerve Regeneration through Longitudinal Nanogrooves on a Fiber Surface. *ACS Applied Materials & Interfaces*, *7*(13), 7189–7196. https://doi.org/10.1021/am509227t

Institute of Chemistry (The Hebrew University of Jerusalem). (2017). What is NMR? Uses of NMR spectrometry. Retrieved August, 2017, from http://chem.ch.huji.ac.il/nmr/whatisnmr/whatisnmr.html

Janke, D., Jankowski, J., Rüth, M., Buschmann, I., Lemke, H.-D., Jacobi, D., … Jankowski, V. (2013). The "Artificial Artery" as In Vitro Perfusion Model. *PloS One*, *8*(3), e57227. https://doi.org/10.1371/journal.pone.0057227

Janmey, P. A., Winer, J. P., & Weisel, J. W. (2009). Fibrin gels and their clinical and bioengineering applications. *Journal of the Royal Society, Interface*, *6*(30), 1–10. https://doi.org/10.1098/rsif.2008.0327

Jha, B. S., Colello, R. J., Bowman, J. R., Sell, S. A., Lee, K. D., Bigbee, J. W., … Simpson, D. G. (2011). Two pole air gap electrospinning: Fabrication of highly aligned, three-dimensional scaffolds for nerve reconstruction. *Acta Biomaterialia*, *7*(1), 203–215. https://doi.org/10.1016/j.actbio.2010.08.004

Jha, A. K., Mathur, A., Svedlund, F. L., Ye, J., Yeghiazarians, Y., & Healy, K. E. (2015). Molecular Weight and Concentration of Heparin in Hyaluronic Acid-based Matrices Modulates Growth Factor Retention Kinetics and Stem Cell Fate. *Journal of Controlled Release : Official Journal of the Controlled Release Society*, 209, 308–316. http://doi.org/10.1016/j.jconrel.2015.04.034

Jin, K. L., Mao, X. O., & Greenberg, D. A. (2000). Vascular endothelial growth factor: direct neuroprotective effect in in vitro ischemia. *Proceedings of the National Academy of Sciences of the United States of America*, *97*(18), 10242–7. Retrieved from http://www.ncbi.nlm.nih.gov/pubmed/10963684

Kalson NS, Lu Y, Taylor SH, Starborg T, Holmes DF, Kadler KE. (2015). A structure-based extracellular matrix expansion mechanism of fibrous tissue growth. *Elife.* May 20;4. Retrieved from: http://www.ncbi.nlm.nih.gov/pubmed/25992598

Kim, J. I., Hwang, T. I., Aguilar, L. E., Park, C. H., & Kim, C. S. (2016). A Controlled Design of Aligned and Random Nanofibers for 3D Bi-functionalized Nerve Conduits Fabricated via a Novel Electrospinning Set-up. *Scientific Reports*, *6*, 23761. https://doi.org/10.1038/srep23761

Kong, B., & Mi, S. (2016). Electrospun Scaffolds for Corneal Tissue Engineering: A Review. *Materials (Basel, Switzerland)*, *9*(8). https://doi.org/10.3390/ma9080614

Laranjeira, M. C. M., & Fávere, V. T. de. (2009). Quitosana: biopolímero funcional com potencial industrial biomédico. *Química Nova*, *32*(3), 672–678. https://doi.org/10.1590/S0100-40422009000300011

Lee, J.-Y., Kim, S.-M., Kim, M.-J., & Lee, J.-H. (2014). Controlled release of nerve growth factor from heparin-conjugated fibrin gel within the nerve growth factor-delivering implant. *Journal of the Korean Association of Oral and Maxillofacial Surgeons*, *40*(1), 3–10. https://doi.org/10.5125/jkaoms.2014.40.1.3

LEV, R., & SPICER, S. S. (1964). Specific Staining of Sulphate Groups with Alcian Blue at low ph PH. *Journal of Histochemistry & Cytochemistry*, *12*(4), 309–309. https://doi.org/10.1177/12.4.309

Lin, C.-C., & Anseth, K. S. (2009). PEG Hydrogels for the Controlled Release of Biomolecules in Regenerative Medicine. *Pharmaceutical Research*, *26*(3), 631–643. https://doi.org/10.1007/s11095-008-9801-2

Lin, W.-C., Liu, T.-Y., & Yang, M.-C. (2004). Hemocompatibility of polyacrylonitrile dialysis membrane immobilized with chitosan and heparin conjugate. *Biomaterials*, *25*(10), 1947–57. Retrieved from http://www.ncbi.nlm.nih.gov/pubmed/14738859

Ma, C., Jing, Y., Sun, H. and Liu, X. (2015). Hierarchical Nanofibrous Microspheres with Controlled Growth Factor Delivery for Bone Regeneration. *Advanced Healthcare Materials*, 4(17), pp.2699-2708. Retrieved from: https://www.ncbi.nlm.nih.gov/pubmed/26462137

Malheiro A, Wieringa P, Mota C, Baker M, Moroni L. (2016). Patterning Vasculature: The Role of Biofabrication to Achieve an Integrated Multicellular Ecosystem. *ACS Biomater Sci Eng.* 10;2(10):1694–709. Retrieved from: http://pubs.acs.org/doi/abs/10.1021/acsbiomaterials.6b00269

Marrella, A., Lee, T., Lee, D., Karuthedom, S., Syla, D., Chawla, A., Khademhosseini, A. and Jang, H. (2017). Engineering vascularized and innervated bone biomaterials for improved skeletal tissue regeneration. *Materials Today*. Retrieved from: http://www.sciencedirect.com/science/article/pii/S1369702117304121

McGraw-Hill Higher Education. (2000). Nuclear Magnetic Resonance. Retrieved August, 2017, from http://www.mhhe.com/physsci/chemistry/carey/student/olc/ch13nmr.html

Moon, J. J., & West, J. L. (2008). Vascularization of engineered tissues: approaches to promote angio-genesis in biomaterials. *Current Topics in Medicinal Chemistry*, *8*(4), 300–10. Retrieved from http://www.ncbi.nlm.nih.gov/pubmed/18393893

Muehleder, S., Ovsianikov, A., Zipperle, J., Redl, H. and Holnthoner, W. (2014). Connections Matter: Channeled Hydrogels to Improve Vascularization. *Frontiers in Bioengineering and Biotechnology*, 2. Retrieved from: http://www.ncbi.nlm.nih.gov/pubmed/25453032

Nanoscience Instruments. (2017). How does Scanning Electron Microscopy work? Retrieved August, 2017, from http://www.nanoscience.com/technology/sem-technology/

Naves, L. B., Dhand, C., Venugopal, J. R., Rajamani, L., Ramakrishna, S., & Almeida, L. (2017). Nanotechnology for the treatment of melanoma skin cancer. *Progress in Biomaterials*, *6*(1–2), 13–26. https://doi.org/10.1007/s40204-017-0064-z

Noori, A., Ashrafi, S. J., Vaez-Ghaemi, R., Hatamian-Zaremi, A., & Webster, T. J. (2017). A review of fibrin and fibrin composites for bone tissue engineering. *International Journal of Nanomedicine*, *12*, 4937–4961. https://doi.org/10.2147/IJN.S124671

Panambur, Gangadhar, Koltover, Ilya, Batcheller, S. (2017). NIPAM based Polymers | Sigma-Aldrich. Retrieved August, 2017, from http://www.sigmaaldrich.com/materials-science/polymer-science/nipam-polymers.html

Papavasiliou, G., Sokic, S., & Turturro, M. (2012). Synthetic PEG Hydrogels as Extracellular Matrix Mimics for Tissue Engineering Applications. *Biotechnology - Molecular Studies and Novel Applications for Improved Quality of Human Life*. InTech. https://doi.org/10.5772/31695

Patra, H. K., Sharma, Y., Islam, M. M., Jafari, M. J., Murugan, N. A., Kobayashi, H., … Tiwari, A. (2016). Inflammation-sensitive in situ smart scaffolding for regenerative medicine. *Nanoscale*, *8*(39), 17213–17222. https://doi.org/10.1039/c6nr06157e

Reinertsen, E., Skinner, M., Wu, B., & Tawil, B. (2014). Concentration of fibrin and presence of plasminogen affect proliferation, fibrinolytic activity, and morphology of human fibroblasts and keratinocytes in 3D fibrin constructs. *Tissue Engineering. Part A*, *20*(21–22), 2860–9. https://doi.org/10.1089/ten.TEA.2013.0423

Rubert, M., Alonso-Sande, M., Monjo, M., & Ramis, J. M. (2012). Evaluation of Alginate and Hyaluronic Acid for Their Use in Bone Tissue Engineering. *Biointerphases*, *7*(1), 44. https://doi.org/10.1007/s13758-012-0044-8

Sapountzi, E., Braiek, M., Chateaux, J.-F., Jaffrezic-Renault, N., & Lagarde, F. (2017). Recent Advances in Electrospun Nanofiber Interfaces for Biosensing Devices. *Sensors (Basel, Switzerland)*, *17*(8). https://doi.org/10.3390/s17081887

Schenone M, Furie BC, Furie B. (2004). The blood coagulation cascade. *Curr Opin Hematol.* Jul;11(4):272-7. Review. PubMed PMID: 15314527. Retrieved from: https://www.ncbi.nlm.nih.gov/pubmed/15314527

Scott, J. E., & Dorling, J. (1965). Differential staining of acid glycosaminoglycans (mucopolysaccharides) by alcian blue in salt solutions. *Histochemie. Histochemistry. Histochimie*, *5*(3), 221–33. Retrieved from http://www.ncbi.nlm.nih.gov/pubmed/4223499

Slaughter, B. V., Khurshid, S. S., Fisher, O. Z., Khademhosseini, A., & Peppas, N. A. (2009). Hydrogels in Regenerative Medicine. *Advanced Materials*, *21*(32–33), 3307–3329. https://doi.org/10.1002/adma.200802106

Starkey, L. S. (2017). NMR Chemical Shifts. Retrieved from https://www.cpp.edu/~lsstarkey/courses/NMR/NMRshifts1H-general.pdf

Steven J. Barnes, L. P. H. (2008). *Tissue Engineering: Roles, Materials, and Applications*. Nova Science Publishers.

Stone, W. L., & Bhimji, S. S. (2017). *Physiology, Growth Factor*. *StatPearls*. StatPearls Publishing. Retrieved from http://www.ncbi.nlm.nih.gov/pubmed/28723053

Straccia, M., d'Ayala, G., Romano, I., Oliva, A., & Laurienzo, P. (2015). Alginate Hydrogels Coated with Chitosan for Wound Dressing. *Marine Drugs*, *13*(5), 2890–2908. https://doi.org/10.3390/md13052890

Synowiecki, J., & Al-Khateeb, N. A. (2003). Production, Properties, and Some New Applications of Chitin and Its Derivatives. *Critical Reviews in Food Science and Nutrition*, *43*(2), 145–171. https://doi.org/10.1080/10408690390826473

Terenghi, G. (1995). Peripheral nerve injury and regeneration. *Histology and Histopathology*, *10*(3), 709–18. Retrieved from http://www.ncbi.nlm.nih.gov/pubmed/7579822

The Federal Institute for Drugs and Medical Devices (BfArM). (2017). Impurity Evaluation of Heparin Sodium by 1 H-NMR Spectroscopy. Retrieved from https://www.bfarm.de/EN/Home/home_node.html

The University of Utah - Physiological Gels Research Group, Mathematical Biology, Department of Mathematics, (2017). Fibrin Formation. Retrieved from: https://www.math.utah.edu/research/mathbio/groups/gels/gel_fibrin_page.html

Thermo Fisher. (2017-a). FTIR Basics. Retrieved from https://www.thermofisher.com/pt/en/home/industrial/spectroscopy-elemental-isotope-analysis/spectroscopy-elemental-isotope-analysis-learning-center/molecular-spectroscopy-information/ftir-information/ftir-basics.html

Thermo Fisher. (2017-b). FTIR Sample Techniques: Attenuated Total Reflection (ATR). Retrieved from https://www.thermofisher.com/pt/en/home/industrial/spectroscopy-elemental-isotope-analysis/spectroscopy-elemental-isotope-analysis-learning-center/molecular-spectroscopy-information/ftir-information/ftir-sample-handling-techniques/ftir-sample-handling-tec

Thermo Fisher. (2017). Overview of ELISA. Retrieved from https://www.thermofisher.com/pt/en/home/life-science/protein-biology/protein-biology-learning-center/protein-biology-resource-library/pierce-protein-methods/overview-elisa.html

Ulery, B. D., Nair, L. S., & Laurencin, C. T. (2011). Biomedical Applications of Biodegradable Polymers. *Journal of Polymer Science. Part B, Polymer Physics*, *49*(12), 832–864. https://doi.org/10.1002/polb.22259

Vacanti, C. A. (2007). Chapter One – The History and Scope of Tissue Engineering. In *Principles of Tissue Engineering* (pp. 3–6). https://doi.org/10.1016/B978-012370615-7/50005-6

Vo, T. N., Kasper, F. K., & Mikos, A. G. (2012). Strategies for controlled delivery of growth factors and cells for bone regeneration. *Advanced Drug Delivery Reviews*, *64*(12), 1292–309. https://doi.org/10.1016/j.addr.2012.01.016

Walter, M. S., Frank, M. J., Rubert, M., Monjo, M., Lyngstadaas, S. P., & Haugen, H. J. (2014). Simvastatin-activated implant surface promotes osteoblast differentiation in vitro. *Journal of Biomaterials Applications*, *28*(6), 897–908. https://doi.org/10.1177/0885328213486364

Weatherall, D., Greenwood, B., Chee, H. L., & Wasi, P. (2006). Science and Technology for Disease Control: Past, Present, and Future. Retrieved from https://www.ncbi.nlm.nih.gov/books/nbk11740/

Willerth, S. M., & Sakiyama-Elbert, S. E. (2008). *Combining stem cells and biomaterial scaffolds for constructing tissues and cell delivery*. *StemBook*. Harvard Stem Cell Institute. https://doi.org/10.3824/stembook.1.1.1

Wongtrakul MD, Saichol, Bishop MD, Allen T., Friedrich, P. F. (2002). Vascular endothelial growth factor promotion of neoangiogenesis in conventional nerve grafts. *The Journal of Hand Surgery*, *27*(2), 277–285. https://doi.org/10.1053/JHSU.2002.31158

Yadav, P., Yadav, H., Shah, V. G., Shah, G., & Dhaka, G. (2015). Biomedical Biopolymers, their Origin and Evolution in Biomedical Sciences: A Systematic Review. *Journal of Clinical and Diagnostic Research : JCDR*, *9*(9), ZE21-5. https://doi.org/10.7860/JCDR/2015/13907.6565

Yan, Q., Xiao, L.-Q., Tan, L., Sun, W., Wu, T., Chen, L.-W., … Shi, B. (2015). Controlled release of simvastatin-loaded thermo-sensitive PLGA-PEG-PLGA hydrogel for bone tissue regeneration: *in vitro* and *in vivo* characteristics. *Journal of Biomedical Materials Research Part A*, *103*(11), 3580–3589. https://doi.org/10.1002/jbm.a.35499

Yang, F., Murugan, R., Wang, S., & Ramakrishna, S. (2005). Electrospinning of nano/micro scale poly(l-lactic acid) aligned fibers and their potential in neural tissue engineering. *Biomaterials*, *26*(15), 2603–2610. https://doi.org/10.1016/j.biomaterials.2004.06.051

Yang, F., Zhao, S., Zhang, F., He, F., & Yang, G. (2011). Simvastatin-loaded porous implant surfaces stimulate preosteoblasts differentiation: an in vitro study. *Oral Surgery, Oral Medicine, Oral Pathology, Oral Radiology, and Endodontology*, *111*(5), 551–556. https://doi.org/10.1016/j.tripleo.2010.06.018

Yang, H. S., La, W.-G., Bhang, S. H., Jeon, J.-Y., Lee, J. H., & Kim, B.-S. (2010). Heparin-Conjugated Fibrin as an Injectable System. *Tissue Engineering Part A*, *16*(4), 1–10. https://doi.org/10.1089=ten.tea.2009.0390

You, I., Kang, S. M., Byun, Y., & Lee, H. (2011). Enhancement of Blood Compatibility of Poly(urethane) Substrates by Mussel-Inspired Adhesive Heparin Coating. *Bioconjugate Chemistry*, *22*(7), 1264–1269. https://doi.org/10.1021/bc2000534

Yu, T. T., & Shoichet, M. S. (2005). Guided cell adhesion and outgrowth in peptide-modified channels for neural tissue engineering. *Biomaterials*, *26*(13), 1507–1514. https://doi.org/10.1016/j.biomaterials.2004.05.012

Zachary, I. (2005). Neuroprotective Role of Vascular Endothelial Growth Factor: Signalling Mechanisms, Biological Function, and Therapeutic Potential. *Neurosignals*, *14*(5), 207–221. https://doi.org/10.1159/000088637

Zhang, W., Ronca, S., & Mele, E. (2017). Electrospun Nanofibres Containing Antimicrobial Plant Extracts. *Nanomaterials (Basel, Switzerland)*, *7*(2). https://doi.org/10.3390/nano7020042

Zhang, Z., Li, B., Suwan, J., Zhang, F., Wang, Z., Liu, H., … Linhardt, R. J. (2009). Analysis of pharmaceutical heparins and potential contaminants using 1H-NMR and PAGE. *Journal of Pharmaceutical Sciences*, *98*(11), 4017–4026. https://doi.org/10.1002/jps.21729

Zhao, H., Wu, J., Zhu, J., Xiao, Z., He, C., Shi, H., … Xiao, J. (2015). Research Advances in Tissue Engineering Materials for Sustained Release of Growth Factors. *BioMed Research International*, *2015*, 808202. https://doi.org/10.1155/2015/808202

Zhao, L., Weir, M. D., & Xu, H. H. K. (2010). An injectable calcium phosphate-alginate hydrogel-umbilical cord mesenchymal stem cell paste for bone tissue engineering. *Biomaterials*, *31*(25), 6502–6510. https://doi.org/10.1016/j.biomaterials.2010.05.017

Zhao, Z., Wang, Y., Peng, J., Qi, H., Zhao, B., Zhang, L., … Lu, S. (2011). [Influence of aligned electrospinning poly (propylene carbonate) on axonal growth of dorsal root ganglion in vitro]. *Journal of Reparative and Reconstructive Surgery*, *25*(2), 171–5. Retrieved from http://www.ncbi.nlm.nih.gov/pubmed/21427845

Zheng, X., Zhang, Q., Liu, J., Pei, Y. and Tang, K. (2016). A unique high mechanical strength dialdehyde microfibrillated cellulose/gelatin composite hydrogel with a giant network structure. *RSC Advances*, 6(76), pp.71999-72007. https://doi.org/10.1039/c6ra12517d

Zuber, M., Zia, K. M., & Barikani, M. (2013). Chitin and Chitosan Based Blends, Composites and Nanocomposites (pp. 55–119). https://doi.org/10.1007/978-3-642-20940-6_3

Appendices

Appendix 1

This text corresponds to the first method designed to obtain Heparin-conjugated Fibrinogen.

30 mg of Heparin were dissolved in a 2-(N-morpholino)ethanesulfonic acid buffer solution (MES, 0.5M, pH 6). N-hydroxysuccinimide (NHS) and 1-ethyl-3-(3-dimethylaminopropyl)-carbodiimide hydrochloride (EDC) were added to the previous solution to have a final concentration of 0.04 mM and 0.08 mM. The solution was left to react for 12 h at 4ºC under agitation for activation of the Heparin's carboxylic acid groups. It was then stirred to obtain a homogeneous solution and precipitated to extract the activated Heparin using excess of acetone anhydride, followed by vacuum dry for 24 h at 20°C. 30 mg were dissolved in 6 ml of warm (at 37ºC) PBS of Fibrinogen. 18 mg of activated Heparin product were added and reacted for 3 h at 4ºC under agitation. The resultant solution was precipitated using excess of acetone anhydride and vacuum dried for 24 h at 20ºC. The dried product was dissolved in Phosphate Buffered Saline (PBS), dialyzed through a porous membrane bag for 24 h at 4ºC (with MilliQ water changes every 2-4 h), and lyophilized for 48 h.

Appendix 2

This appendix has the purpose of describing how the carbodiimide chemistry works and important crosslinking remarks related to this thesis work.

Crosslinking: it is the process of chemically joining two or more molecules by a covalent bond. Functional groups (primary amines, etc.) on proteins or other molecules are found to be reactive with specific crosslinking reagents ends. Chemical groups become targets for conjugation and for study using crosslinking methods because of their availability in proteins and peptides. This area of chemistry is known as bioconjugation and includes not only crosslinking processes, but also immobilization procedures, surface modifications and labeling of biomolecules.

The reactive chemical group: the most important property of a crosslinker is its reactive chemical group, since it establishes the method and mechanism for chemical modification. At least two reactive groups are found in crosslinkers and, as previously mentioned, these target common functional groups found in biomolecules such as proteins and nucleic acids. The functional groups that are commonly targeted for bioconjugation include primary amines, carbohydrates, sulfhydryls, carbonyls and carboxylic acids.

Carboxylic acid-reactive chemical groups: carboxylic acids (–COOH) exist in the side chains of aspartic acid (Asp, D) and glutamic acid (Glu, E), and at the C-terminus of each polypeptide chain. Carboxylic acids are reactive towards carbodiimides.

Carbodiimides: EDC and other carbodiimides cause direct conjugation of carboxylates (–COOH) to primary amines (–NH2) without becoming part of the final amide-bond crosslink between target molecules. Direct EDC-mediated crosslinking usually causes random polymerization of polypeptides because peptides and proteins contain multiple carboxyls and amines. Nevertheless, this reaction is widely used in immunogen preparation (e.g., attaching a large carrier protein to a small peptide), and in immobilization procedures (e.g., attaching proteins to a carboxylated surface).

EDC reaction: an active O-acylisourea intermediate is formed by the reaction of EDC with carboxylic acid groups. This intermediate is easily displaced by nucleophilic attack from primary amino groups in the reaction mixture. The original carboxyl group forms an amide bond with the primary amine, and an EDC by-product is released as a soluble urea derivative. In aqueous solutions, the O-acylisourea intermediate is unstable, and if the reaction with an amine fails, it will result in the regeneration of the carboxyls, the hydrolysis of the intermediate, and the release of an N-unsubstituted

urea. EDC crosslinking is most efficient and must be performed in acidic (pH 4.5) buffer conditions with no extra possession of carboxyls and amines. A suitable carbodiimide reaction buffer is MES (4-morpholinoethanesulfonic acid). In addition, phosphate buffers and neutral pH (up to 7.2) conditions are also compatible with the reaction chemistry, but present lower efficiency values. However, increasing the amount of EDC in a reaction solution can compensate for the reduced efficiency (Thermo Fisher Scientific Inc., 2012).

EDC and Sulfo-NHS reaction: N-hydroxysuccinimide (NHS) or its water-soluble analog (sulfo-NHS) are often included in EDC coupling procedures to create dry-stable (amine-reactive) intermediates or to improve efficiency process efficiency (Fig. 30).

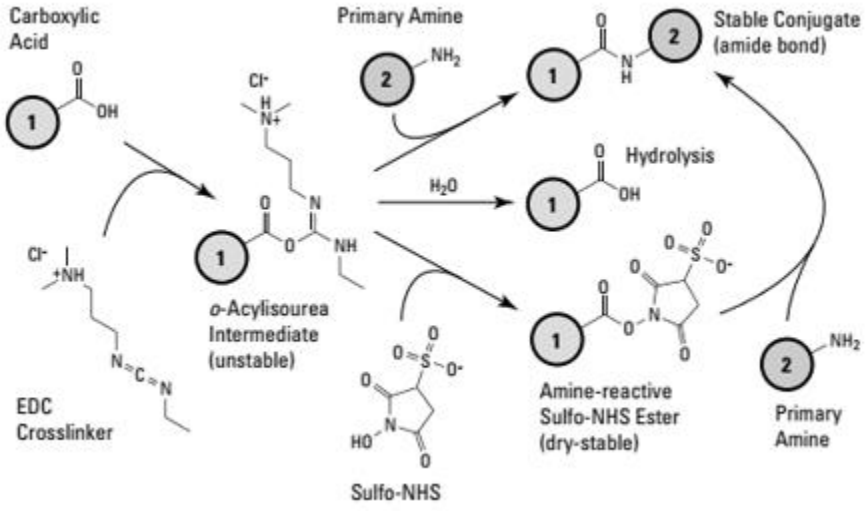

Fig. 30. Sulfo-NHS plus EDC (carbodiimide) crosslinking reaction scheme: carboxyl-toamine crosslinking using the carbodiimide EDC and Sulfo-NHS. Addition of NHS or Sulfo-NHS to EDC reactions increases efficiency and enables specific molecule (1) to be activated. From (Thermo Fisher Scientific Inc., 2012).

In comparison to normal EDC reaction, EDC with NHS form a coupling with carboxyls, presenting an NHS ester that is considerably more stable than the O-acylisourea intermediate, while allowing efficient conjugation to primary amines at physiologic pH.

Activation of heparin: according to literature, EDC/NHS can activate carboxyl acid groups of the heparin and promote their covalent binding to amino groups; which has been proved to be non-cytotoxic (You, Kang, Byun, & Lee, 2011) and biocompatible (Elahi, Guan, Wang, & King, 2014; W.-C. Lin, Liu, & Yang, 2004).

Appendix 3

This appendix has the purpose of describing how the Nuclear Magnetic Resonance (NMR) works and important remarks related to this thesis work.

The NMR spectroscopy is an analytical chemistry technique used for determining the content, molecular structure and purity of a sample (Institute of Chemistry, The Hebrew University of Jerusalem, 2017). Mixtures containing known compounds can be quantitatively analyzed by NMR. For unknown compounds, NMR can also analyze them by finding matches against spectral libraries or to infer the basic structure directly. Once the basic structure is known, the molecular conformation in solution can also be determined by NMR as well as studying physical properties at the molecular level, such as phase changes, solubility, diffusion, among others.

The principle of NMR is that many nuclei have spin and all nuclei are electrically charged. An energy transfer is possible between the base energy to a higher energy level (generally a single energy gap) if an external magnetic field is applied. The energy transfer takes place at a wavelength that corresponds to radio frequencies, and the energy is emitted at the same frequency once the spin returns to its base level. The signal that matches this transfer is measured in many ways and processed in order to yield an NMR spectrum for the nucleus in concern (McGraw-Hill Higher Education, 2000).

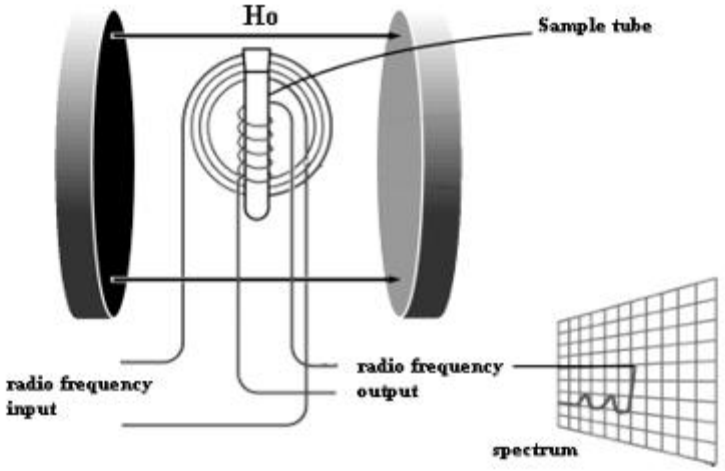

Fig. 31. Schematic of NMR spectrometer sample handling and spectrum output. From (McGraw-Hill Higher Education, 2000).

The sample is positioned in the magnetic field and excited via pulsations in the radio frequency input circuit. A radio signal in the output circuit is induced by the realigned magnetic fields, and it is used to generate the output signal. Fourier analysis of the complex output produces the actual spectrum.

To allow the signals to be identified from the background noise, the pulse is repeated as many times as necessary (McGraw-Hill Higher Education, 2000).

The chemical shift

- An NMR spectrum is a plot of the radio frequency applied against absorption.
- Resonance is the signal in the spectrum.
- The frequency of a signal is referred to as a chemical shift.

In absolute terms, the chemical shift is defined by the frequency of the resonance expressed with reference to a standard compound which is defined to be at 0 ppm.

$$Chemical\ shift\ (\delta) = \frac{frequency\ of\ signal - frequency\ of\ reference}{spectrometer\ frequency} \times 10^6$$

Equation 1. Chemical shift of NMR

By expressing it in parts per million (ppm), the scale is made more manageable and is independent of the spectrometer frequency. In this way, it is more convenient to describe the relative positions of the resonances in an NMR spectrum. The following chemical shift sheet was used in order to analyze the NMR spectrum (Fig. 32).

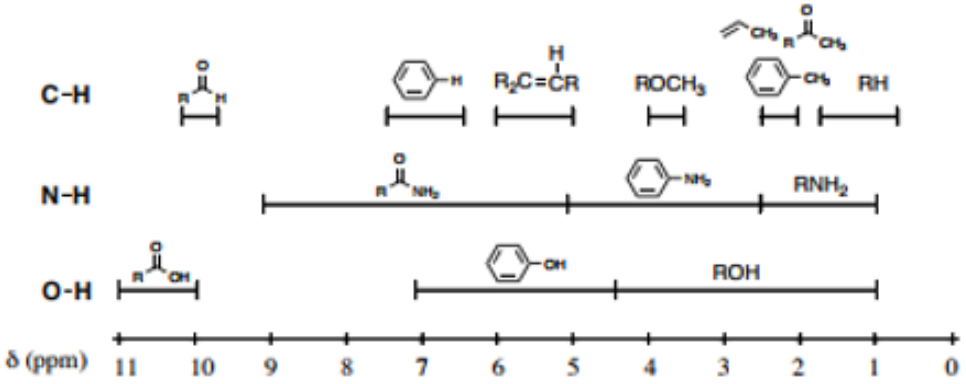

Protons on Carbon

ype of C-H	δ (ppm)	Description of Proton
R–CH_3	0.9	alkyl (methyl)
–CH_2–R	1.3	alkyl (methylene)
R_3C–H	1.5-2	alkyl (methine)
	1.8	allylic (C is next to a pi bond)
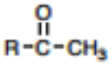	2-2.3	α to carbonyl (C is next to C=O)
Ar–CH_3	2.3	benzylic (C is next to Ph)
RC≡C–H	2.5	alkynyl
R_2N–CH_3	2-3	α to nitrogen (C is attached to N)
R–CH_2–X	2-4	α to halogen (C is attached to Cl, Br, I)
RO–CH_3	3.8	α to oxygen (C is attached to O)
R–CH_2–F	4.5	α to fluorine (C is attached to F)
	5-5.3	vinylic (H is attached to alkene C)
Ar–H	7.3	aromatic (H is on phenyl ring)
	9.7	aldehyde (H is on C=O)

Note: aldehyde (-CHO) proton usually does not couple with neighboring H's so appears as a singlet

Protons on Oxygen/Nitrogen*

Type of H	δ (ppm)	Description
ROH	0.5-5	alcohol
ArOH	4-7	phenol
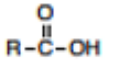	10-13	carb. acid
RNH_2	0.5-5	amine
$ArNH_2$	3-5	aniline
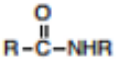	5-9	amide

**Protons on N or O typically have wide ranges of expected chemical shifts; the actual δ value depends on the solvent used, the concentration, temperature, etc. Because these protons are acidic and, therefore, exchangeable, they may be broad peaks and usually do not couple with neighboring protons (typically they are broad singlets). If a protic deuterated solvent is used (e.g., D_2O or CD_3OD), then the NH and OH protons will exchange with the deuterium and the peaks will shrink or disappear entirely, since D (^2H) does not show up in the ^1H NMR spectrum.*

R = alkyl group
Ar = aromatic ring, such as phenyl (Ph)

Fig. 32. NMR Chemical Shifts sheet. From (Starkey, 2017).

Appendix 4

This appendix has the purpose of describing how the Fourier-transform infrared spectroscopy (FTIR) works and important remarks related to this thesis work.

FTIR is an infrared spectroscopy method where some IR radiation is passed through a sample and absorbed, and/or transmitted (Thermo Fisher Scientific Inc., 2017a). The resulting signal at the detector is a spectrum representing a molecular "fingerprint" of the sample. This is useful since different chemical structures (molecules) produce different spectral fingerprints. Hence, structural insights from the samples can be obtained.

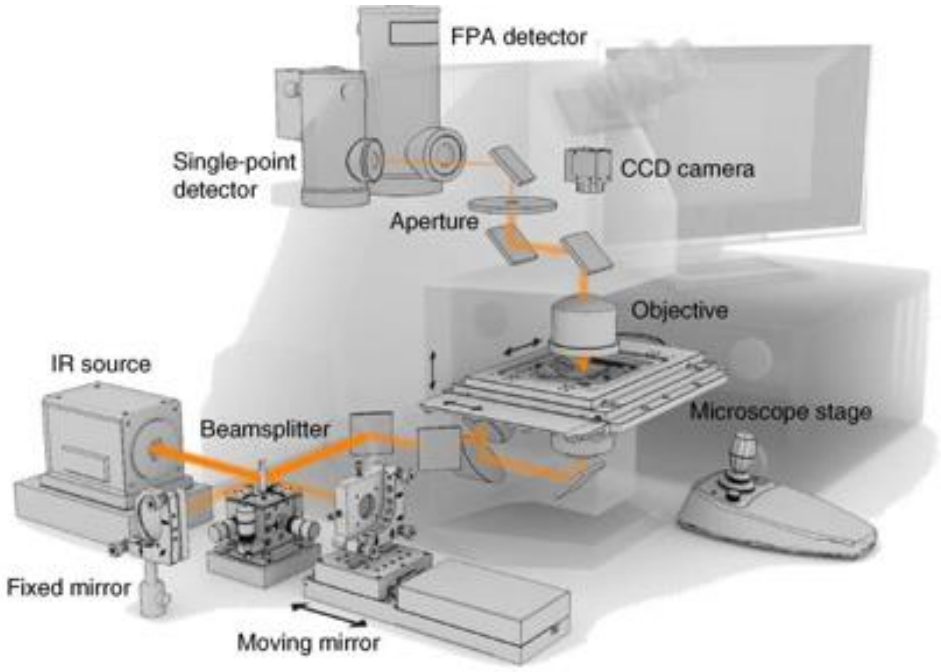

Fig. 33. Schematic of FTIR spectrometer. From (Baker *et al.*, 2014).

There are four major IR-spectroscopic sampling techniques: transmission, specular reflection, diffuse reflectance and attenuated total reflection (ATR). In this thesis work, the samples were solid, and hence, this was the ideal technique since the samples could be analyzed with a diamond ATR-crystal which possessed extreme chemical and mechanical robustness. The technique worked well for these samples because the intensity of the evanescent waves decays exponentially with distance from the surface of the ATR crystal, making the technique generally insensitive to the solid samples' thickness. When the beam comes into contact with a sample, the ATR accessory operates by measuring the changes that occur in an internally reflected IR beam (Fig. 34).

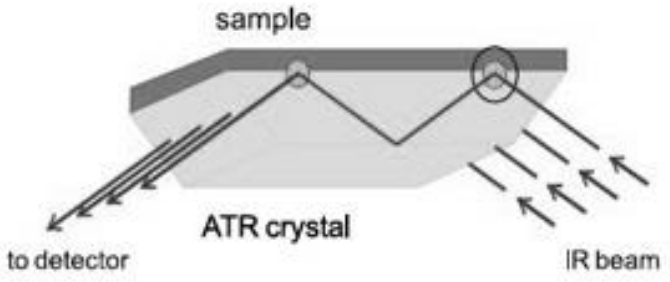

Fig. 34. ATR principle. From (Bruker Optics, 2012).

The infrared beam will enter the ATR crystal at an angle, relative to the crystal surface, of typically 45° and will be totally reflected at the crystal to sample interface. The fraction of light reaching into the sample is known as evanescent wave. Its penetration depth depends on the wavelength, the refractive indices of the ATR crystal, the sample and the angle of the entering light beam. The evanescent wave will be attenuated in the spectral regions where the sample absorbs energy. The attenuated beam will return to the crystal, then exits the opposite end of the crystal and be directed to the detector in the IR spectrometer. The detector will record the received IR beam as a signal, which will be used to generate the IR spectrum (Thermo Fisher Scientific Inc., 2017b).

Appendix 5

This appendix has the purpose of describing how the Scanning Electron Microscopy (SEM) works and important remarks related to this thesis work.

Many structures can no longer be characterized by light microscopy, since nowadays, for several reasons, materials and devices are shrinking and going towards smaller dimensions. The electron microscope was developed when the wavelength became the limiting factor in light microscopes. Electrons enable better resolutions since they have much shorter wavelengths (Nanoscience Instruments, 2017).

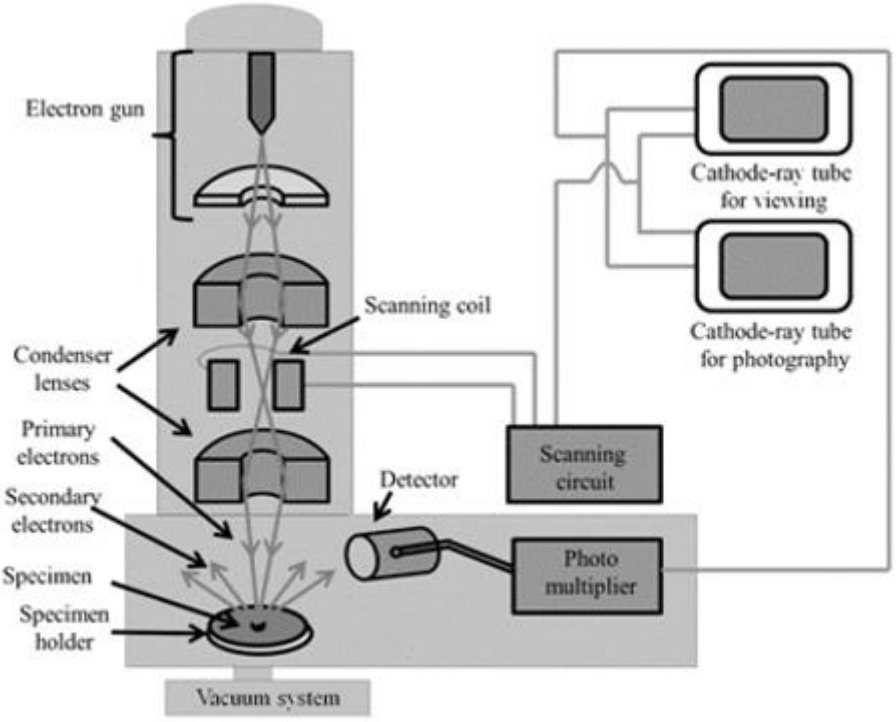

Fig. 35. Schematic of a scanning electron microscope. From (National Programme on Technology Enhanced Learning, 2017).

SEM uses an electron gun that generates a beam of high energy electrons, processed by magnetic lenses, focused at the specimen surface and systematically scanned ("rastered") across the surface of a specimen. The electrons in a scanning electron microscope never form a real image of the sample, unlike the light in a light microscope. The SEM image is an electronic image, it is in the form of a serial data stream. This is the result of the beam probe illuminating the sample in a rectangular scanning pattern (raster) one point at a time, with the strength of the signal generated from each point being a reflection of differences (e.g. topographical or compositional) in the sample (Australian Microscopy and

Microanalysis Research Facility, 2013). In a one-to-one relationship between points on the specimen and points on the image viewing screen, the screen is scanned in synchrony with the beam on the specimen. Increased magnification is produced by decreasing the size of the scanned area (Australian Microscopy and Microanalysis Research Facility, 2013).

Sputter coating

Sputter coating for SEM is the process of applying an ultra-thin coating of electrically-conducting metal over poorly or non-conducting conducting specimen. Examples of the metal could be gold (Au), gold/palladium (Au/Pd), silver (Ag), chromium (Cr), iridium (Ir) or platinum (Pt) (Höflinger, 2013). Sputtered films for SEM typically have a thickness range of 2–20 nm. Because of the accumulation of static electric fields, charging of the specimen could occur. To prevent this, the sputter coating process should be performed. The signal to noise ratio can also be increased with SEM by increasing the number of secondary electrons that can be detected from the surface of the specimen.

In general, the general advantages for SEM samples that are sputtered with metal are:

- Increasing of thermal conduction;
- Improvement of secondary electron emission;
- Reduction of microscope beam damage;
- Reduction of sample charging (increased conduction);
- Reduction of beam penetration with improved edge resolution, and
- Protection of beam sensitive specimens (Höflinger, 2013).

Appendix 6

This appendix has the purpose of describing how the ELISA (enzyme-linked immunosorbent) assay works and important remarks related to this thesis work.

ELISA (enzyme-linked immunosorbent assay) is a plate-based assay technique that detects and quantifies substances such as antibodies, proteins, peptides and hormones. The principle of ELISA is that an antigen must be immobilized to a solid surface, and complexed with an antibody that is linked to an enzyme. The detection consists in assessing the conjugated enzyme activity through the incubation with a substrate to produce a measurable product. The most crucial characteristic of the detection step is a highly specific antibody-antigen interaction (Thermo Fisher Scientific Inc., 2017c). Generally, the assay begins with a coating step, where the first layer, either an antigen or an antibody, is adsorbed to a well in an ELISA plate. Coating is followed by blocking and detection steps. Several washes are repeated between each ELISA step to remove unbound materials, since the assay uses surface binding for separation. During this process, to prevent the dilution of the solutions added in the next phase, the removal of excess liquid is essential (Bio-Rad, 2017a).

In general, ELISAs can be grouped into four main categories: direct, indirect, sandwich, and competitive ELISAs. In this thesis work, the sandwich ELISA procedure was used. The advantages of a sandwich ELISA are its high sensitivity, and delivery of high specificity as two antibodies are used to detect the antigen. It offers flexibility since both direct and indirect methods can be used. Sandwich ELISAs require the use of matched antibody pairs composed by the capture and the detection antibodies. Therefore, each antibody is specific for a different and non-overlapping region or epitope of the antigen. Matched antibody pairs should be tested specifically in sandwich ELISA to ensure that they detect different epitopes. This is very important in order to achieve accurate results. The capture antibody, as its name implies, will bind the antigen to later be detected in a direct or in an indirect ELISA configuration (Bio-Rad, 2017).

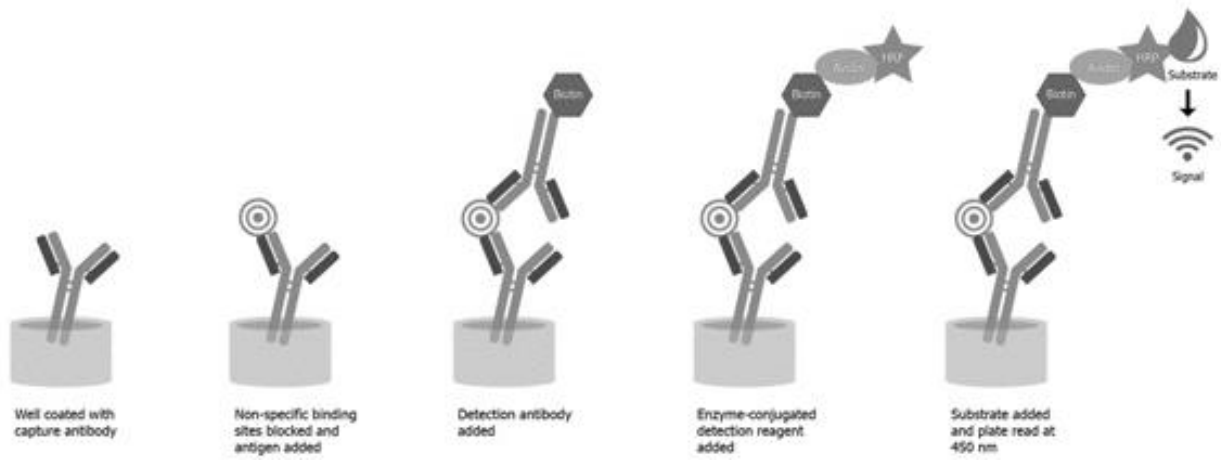

Fig. 36. Overview of a sandwich ELISA. From (Rockland Immunochemicals, 2017).

The sandwich ELISA process begins with a well of the ELISA plate to be coated with a capture antibody (Fig. 36). The sample is then added, followed by a detection antibody. If the detection antibody can be enzyme conjugated, then this is referred to as a direct sandwich ELISA. Indirect sandwich ELISA is when a secondary enzyme-conjugated detection antibody is required because the detection antibody used is unlabeled. Since the antigen does not need to be purified prior to the assay and it still delivers high sensitivity and specificity, sandwich ELISAs seem to be more suited to the analysis of complex samples (Bio-Rad, 2017).

Appendix 7

This appendix has the purpose of describing how the used staining methods (alcian blue, DMMB, phalloidin and DAPI) work and important remarks related to this thesis.

Alcian blue is a group of polyvalent basic dyes that are water soluble and it was used for heparin's detection because it is a known staining assay of acidic GAGs that are carboxylated or sulfated. It stains both sulfated and carboxylated acid glycosaminoglycans and sulfated and carboxylated glycoproteins (LEV & SPICER, 1964; Scott & Dorling, 1965). The blue color is due to the presence of copper in the molecule. The staining reaction happens because Alcian blue forms salt linkages with the acid groups of acid mucopolysaccharides.

The dye 1,9-dimethylmethylene (DMMB) is a thiazine chromotrope agent that presents a change in the absorption spectrum due to the resulting color of the stain becoming different from the color of the dye solution when bound to sulfated GAGs. This fact enables the detection of GAGs in solution (Whitley *et al.*, 1989; Chandrasekhar *et al.*, 1987; Farndale *et al.*, 1982), and that is why this method is widely known and used for GAGs staining.

Phalloidin is a bicyclic peptide that is made from a deadly mushroom named "Death Cap" (Amanita phalloides). It has a high-affinity for F-actin, a linear polymer microfilament found in almost all eukaryotic cells, driving many cellular processes including cell motility and muscle contraction. Phalloidin binds to actin at the junction between subunits (Barden *et al.*, 1987; Faulstich *et al.*, 1993; Steinmetz *et al.*, 1998). It is a convenient probe for labeling, identifying, quantitating, and stabilizing F-actin in fixed and permeabilized cell cultures, tissue sections or cell-free experiments.

Finally, 4',6-diamidino-2-phenylindole (DAPI) is a popular nuclear and chromosome counterstain which forms fluorescent complexes with natural double-stranded DNA, showing a fluorescence specificity for AT, AU and IC clusters. When bound to double-stranded DNA, DAPI has an absorption maximum at a wavelength of 358 nm (ultraviolet) and its emission maximum is at 461 nm (blue). Therefore, for fluorescence microscopy DAPI is excited with ultraviolet light and is detected through a blue/cyan filter.

Appendices' References

Australian Centre for Microscopy & Microanalysis (AMMRF). (2013). SEM Layout | MyScope. Retrieved August, 2017, from http://www.ammrf.org.au/myscope/sem/practice/principles/layout.php

Baker, M. J., Trevisan, J., Bassan, P., Bhargava, R., Butler, H. J., Dorling, K. M., … Martin, F. L. (2014). Using Fourier transform IR spectroscopy to analyze biological materials. *Nature Protocols*, *9*(8), 1771–91. https://doi.org/10.1038/nprot.2014.110

Bio-Rad. (2017)a. ELISA Procedure. Retrieved August, 2017, from https://www.bio-rad-antibodies.com/elisa-procedure.html

Bio-Rad. (2017)b. Types of ELISA. Retrieved August, 2017, from https://www.bio-rad-antibodies.com/elisa-types-direct-indirect-sandwich-competition-elisa-formats.html#Sandwich

Bruker Optics. (2012). ATR: Advantages for FT-IR Spectroscopy. Retrieved August, 2017, from https://www.azom.com/article.aspx?ArticleID=5958

Elahi, M. F., Guan, G., Wang, L., & King, M. W. (2014). Influence of Layer-by-Layer Polyelectrolyte Deposition and EDC/NHS Activated Heparin Immobilization onto Silk Fibroin Fabric. *Materials 7*(4), 2956–2977. https://doi.org/10.3390/ma7042956

Frazier, S. B., Roodhouse, K. A., Hourcade, D. E., & Zhang, L. (2008). The Quantification of Glycosaminoglycans: A Comparison of HPLC, Carbazole, and Alcian Blue Methods. *Open Glycoscience*, *1*(1), 31–39. https://doi.org/10.2174/1875398100801010031

Höflinger, G. (2013, August). Brief Introduction to Coating Technology for Electron Microscopy, Leica-microsystems. Retrieved from http://www.leica-microsystems.com/science-lab/brief-introduction-to-coating-technology-for-electron-microscopy/

Institute of Chemistry, The Hebrew University of Jerusalem (2017). What is NMR? Uses of NMR spectrometry. Retrieved August 2017, from http://chem.ch.huji.ac.il/nmr/whatisnmr/whatisnmr.html

James, T. L. (1998). Fundamentals of NMR. Retrieved August 2017, from http://qudev.ethz.ch/content/courses/phys4/studentspresentations/nmr/James_Fundamentals_of_NMR.pdf

Lev, R., & Spicer, S. S. (1964). Specific staining of sulphate groups with alcian blue at low pH. *Journal of Histochemistry & Cytochemistry*, 12(4), 309–309. https://doi.org/10.1177/12.4.309

McGraw-Hill Higher Education. (2000). Nuclear Magnetic Resonance. Retrieved August 2017, from http://www.mhhe.com/physsci/chemistry/carey/student/olc/ch13nmr.html

Nanoscience Instruments. (2017). How does Scanning Electron Microscopy work? Retrieved August 2017, from http://www.nanoscience.com/technology/sem-technology/

National Programme on Technology Enhanced Learning (NPTEL). (2017). Electron Microscopy-I, Microscopic Methods. Retrieved August 2017, MHRD Project, Indian Gov. from http://nptel.ac.in/courses/102103047/module6/lec34/1.html

Scott, J. E., & Dorling, J. (1965). Differential staining of acid glycosaminoglycans (mucopolysaccharides) by alcian blue in salt solutions. *Histochemie. Histochemistry. Histochimie*, *5*(3), 221–33.

Starkey, L. S. (2017). NMR Chemical Shifts. Retrieved from https://www.cpp.edu/~lsstarkey/courses/NMR/NMRshifts1H-general.pdf

Thermo Fisher Scientific Inc. (2012). *Crosslinking Technical Handbook.* Retrieved from https://tools.thermofisher.com/content/sfs/brochures/1602163-Crosslinking-Reagents-Handbook.pdf

Thermo Fisher Scientific Inc. (2017)a. FTIR Basics. Retrieved from https://www.thermofisher.com/pt/en/home/industrial/spectroscopy-elemental-isotope-analysis/spectroscopy-elemental-isotope-analysis-learning-center/molecular-spectroscopy-information/ftir-information/ftir-basics.html

Thermo Fisher Scientific Inc. (2017)b. FTIR Sample Techniques: Attenuated Total Reflection (ATR). Retrieved from https://www.thermofisher.com/pt/en/home/industrial/spectroscopy-elemental-isotope-analysis/spectroscopy-elemental-isotope-analysis-learning-center/molecular-spectroscopy-information/ftir-information/ftir-sample-handling-techniques/ftir-sample-handling-tec

Thermo Fisher Scientific Inc. (2017)c. Overview of ELISA. Retrieved from https://www.thermofisher.com/pt/en/home/life-science/protein-biology/protein-biology-learning-center/protein-biology-resource-library/pierce-protein-methods/overview-elisa.html

Whiteman, P. (1973). The quantitative measurement of Alcian Blue-glycosaminoglycan complexes. *The Biochemical Journal*, *131*(2), 343–50.